CHARACTERIZATION OF BALLAST STONES FROM THE WRECK SITE AT TRIAL ROCKS

MTD Wingate, Y Lu, IOH Fielding, R Maas, RH Smithies and SEM Gain

CHARACTERIZATION OF BALLAST STONES FROM THE WRECK SITE AT TRIAL ROCKS

MTD Wingate, Y Lu, IOH Fielding, R Maas[1], RH Smithies and SEM Gain[2]

1 School of Earth Sciences, University of Melbourne, Parkville VIC 3010
2 ARC Centre of Excellence for Core to Crust Fluid Systems (CCFS) and GEMOC, Earth and Environmental Sciences, Macquarie University, New South Wales 2109, Australia

PERTH 2022

Geological Survey of Western Australia

MINISTER FOR MINES AND PETROLEUM
Hon Bill Johnston MLA

DIRECTOR GENERAL, DEPARTMENT OF MINES, INDUSTRY REGULATION AND SAFETY
Richard Sellers

EXECUTIVE DIRECTOR, GEOLOGICAL SURVEY AND RESOURCE STRATEGY
Michele Spencer

John de Laeter Centre

THE UNIVERSITY OF MELBOURNE

EXPLORATION INCENTIVE SCHEME

Cover image: Journey to the centre of the Kimberley (© 2010 PL Schubert)

Contents

Figures

Table

Appendices

Characterization of ballast stones from the wreck site at Trial Rocks

MTD Wingate, Y Lu, IOH Fielding, R Maas[1], RH Smithies and SEM Gain[2]

Abstract

The *Trial* was a ship of the English East India Company that left Plymouth, England, in September 1621, bound for the East Indies. On 25 May 1622, the ship struck rocks and sank off the northwest coast of Western Australia. A wreck thought to be the *Trial* was located at Trial Rocks in 1969 but has not been identified unequivocally. Twenty-three ballast stones recovered from the wreck site were provided by the Western Australian Museum to the Geological Survey of Western Australia (GSWA) to determine whether they are likely to have originated from Plymouth or nearby rocks in southwestern England.

The ballast stones are lithologically similar to Lower to Middle Devonian sandstone and siltstone of the Dartmouth and Meadfoot Groups exposed in Plymouth Sound and other parts of southwestern England. The stones consist of siltstone and feldspathic sandstone, and their precursor sediments were probably sourced mainly from nearby granitic rocks. All samples examined are rich in biotite, which is interpreted as mainly detrital, although some could have been redistributed during diagenesis. The high biotite content of the ballast stones is unusual, but not unknown, in sandstones of southwestern England.

U–Pb geochronology of detrital zircons in one ballast stone sample indicates a youngest age component at c. 580 Ma, which is an acceptable maximum depositional age for Devonian rocks in southwestern England. The age spectrum is dominated by distinctive Neoproterozoic components and minor older Paleoproterozoic and late Archean components, which are broadly consistent with data for several peri-Gondwana terranes, such as Avalonia and Armorica. Consistent geochemical and isotopic compositions suggest a sedimentary provenance dominated by igneous rocks, and derivation of the ballast stones from a single sedimentary unit. The Sm–Nd isotope results for three ballast stones are also an excellent match with data for Paleozoic sedimentary rocks in southwestern England, including the Meadfoot Group.

The ballast stones share many characteristics with sedimentary rocks in Plymouth and southwestern England. There are few other rocks in Britain that could have been sources of the ballast stones, and none is located close to a port engaged in shipbuilding in the early 1600s. Based on the results of this study, an origin for the ballast stones in Plymouth Sound or the surrounding area cannot be ruled out. However, several localities in western Europe are possible sources of the ballast stones, and some, such as Porto in Portugal, also have a long maritime history.

KEYWORDS: geochemistry, geochronology, isotope geology, marine archeology, Paleozoic, petrography

Introduction

The *Trial* (or *Tryall*) was a ship of the English East India Company that left Plymouth, England, in September 1621, under the command of Captain John Brookes, to sail to the East Indies (Green, 1977). On 25 May 1622, the ship struck uncharted submerged rocks about 16 km northwest of the northernmost tip of the Montebello Islands, north of Barrow Island, Western Australia. The crew of the *Trial* are believed to have been the first Englishmen to sight or land on Australia, and the wreck to be Australia's oldest known shipwreck.

A wreck thought to be the *Trial* was located at Trial Rocks (Fig. 1) by divers in 1969 and was first investigated by the Western Australian Museum in 1971. Several cannon, anchors, small objects, and 'a considerable quantity of granite ballast' were among artefacts identified at the wreck site (Green, 1977). Although documentary evidence indicates that Trial Rocks is the site of the wreck of the *Trial*, and circumstantial evidence suggests that the wreck is the *Trial*, no items have been found that enable a positive identification.

Twenty-three ballast stones recovered from the wreck site were provided to the Geological Survey of Western Australia (GSWA) for geological characterization, to determine whether they are likely to have originated from rocks in southwestern England, particularly in Plymouth, from where the *Trial* set sail. Equally important would be to potentially rule out a source in that region, which would be evidence that the ship is not the *Trial*.

Several techniques were employed to characterize the ballast stones. Detailed petrography of four samples was conducted to establish characteristics that can be compared with those of possible source rocks. U–Pb geochronology of detrital zircons in one sample yielded an age spectrum, which is like a 'fingerprint' that indicates the ages of zircons present in the source(s) of the sedimentary precursor.

1 School of Earth Sciences, University of Melbourne, Parkville VIC 3010
2 ARC Centre of Excellence for Core to Crust Fluid Systems (CCFS) and GEMOC, Earth and Environmental Sciences, Macquarie University, New South Wales 2109, Australia
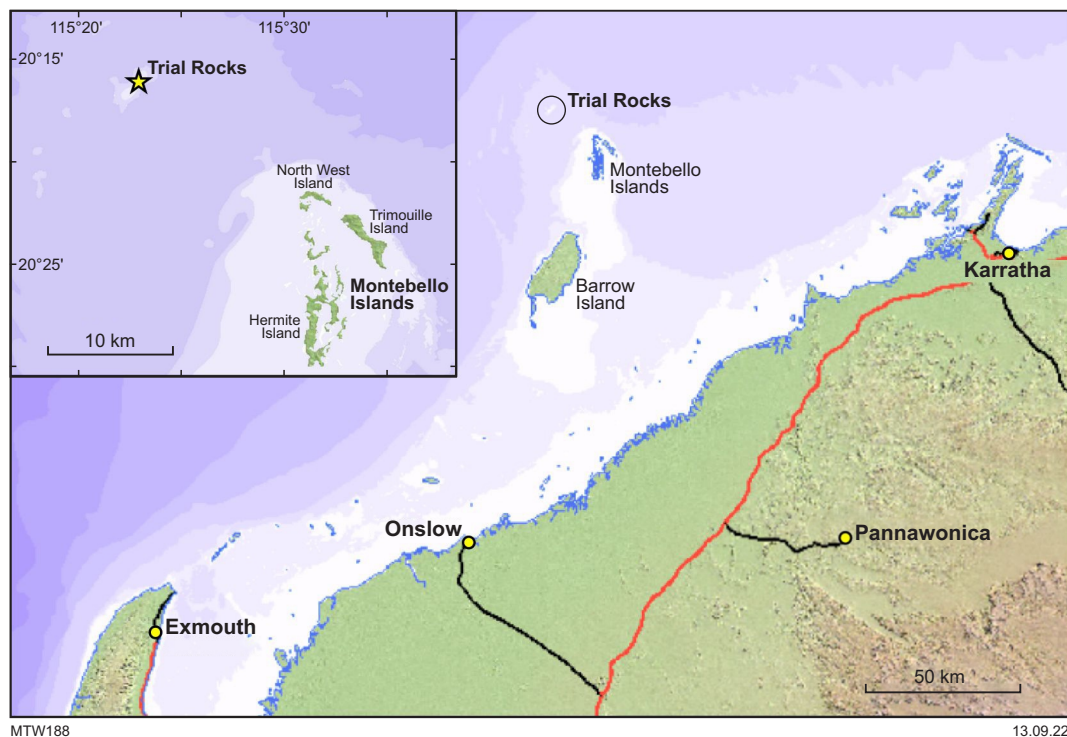
Figure 1. Location of Trial Rocks, north of the Pilbara coast, northwestern Western Australia

Whole-rock lithogeochemistry and samarium–neodymium (Sm–Nd) isotope measurements were undertaken to identify distinctive compositions that might help in matching the ballast stones with possible sources.

Petrography

The 23 ballast stones are pale to dark grey or greenish-grey and fine-grained (Figs 2, 3), and were described previously as 'fine grey granite' (Green, 1977). Visual examination with a hand lens identified most of the stones as fine-grained sedimentary rocks, although several were considered initially to possibly be fine-grained igneous rocks. Subsequent examination of petrographic thin sections, however, showed clearly that all the stones are sedimentary, composed of siltstone or fine-grained sandstone. Nine polished thin sections were prepared from eight ballast stones, and detailed petrographic descriptions are provided in Appendix 1 for four samples (Fig. 3), and summarized in Table 1.

Although most of the stones possess angular, broken surfaces, several are strongly rounded, indicating they were collected from a river bed or ocean beach. Some stones contain mm-scale quartz veins, and one (TR3211-15, Figs 2, 3) is broken along a quartz–chlorite(?) vein at least 1.5 cm thick. Some stones show pale alteration, apparently along joints (e.g. TR3211-15 and -21 in Fig. 2; T003-22 in Fig. 3), and some exhibit planar bedding (e.g. T002-23 in Fig. 3, and TR3211-1 in Appendix 1).

All four samples examined in detail contain mainly angular to sub-angular quartz and feldspar grains (e.g. Fig. 4), abundant biotite and lesser muscovite, and minor ilmenite, and their provenance is interpreted as granitic. Two sandstone samples (TR3211-14 and T002-23) are matrix-poor, moderately sorted, may be weakly deformed, and their mica content is interpreted as mainly detrital, although

some could have been redistributed during diagenesis. Where micas are less abundant, detrital feldspar and quartz grains form a relatively closely packed aggregate. A siltstone (TR3211-12) and a matrix-rich sandstone–siltstone (TR3211-1) may also be weakly deformed, or at least compacted, and contain micas interpreted as mainly detrital.

U–Pb zircon geochronology

Sandstone sample T002-23 was selected for detrital zircon geochronology based on petrographic observations of heavy mineral layers, which include ilmenite and abundant zircon. U–Pb measurements were conducted using the sensitive high-resolution ion microprobe (SHRIMP) facilities at the John de Laeter Centre, Curtin University. Analytical details are provided in Appendix 2 and data are compiled in Appendix 3.

Zircons isolated from the sample are colourless to dark brown, anhedral to euhedral, up to 200 μm long, and equant to elongate, with aspect ratios up to 5:1 (Fig. 5). The crystals are variably rounded, some have pitted outer surfaces and, in cathodoluminescence (CL) images, concentric zoning is truncated at grain boundaries; all features consistent with abrasion during sedimentary transport (Fig. 6).

During the session, 113 zircons were analysed, and measured compositions are mostly concordant (Fig. 7). Nine analyses >1000 Ma and >5% discordant are not considered reliable, and one analysis of a very high-uranium zircon (2925 ppm ^{238}U) yields a 207-corrected ^{238}U/^{206}Pb* date (Pb* = radiogenic Pb) of 488 ± 4 Ma (1σ), interpreted to reflect loss of radiogenic Pb (Fig. 7). The remaining 103 analyses indicate ^{238}U concentrations of 42–1812 ppm (median 291 ppm), ^{232}Th concentrations of 19–1062 ppm (median 135 ppm), and Th/U ratios of 0.03 – 2.34 (median 0.59), and yield ^{207}Pb*/^{206}Pb* or ^{238}U/^{206}Pb* dates of 2804–549 Ma.

Figure 2. Ballast stones TR3211-1 to -21 recovered from the Trial Rocks shipwreck site. Specimens TR3211-5 and -9 are parts of the same ballast stone. Most stones are covered in biogenic material acquired during their residence on the sea floor
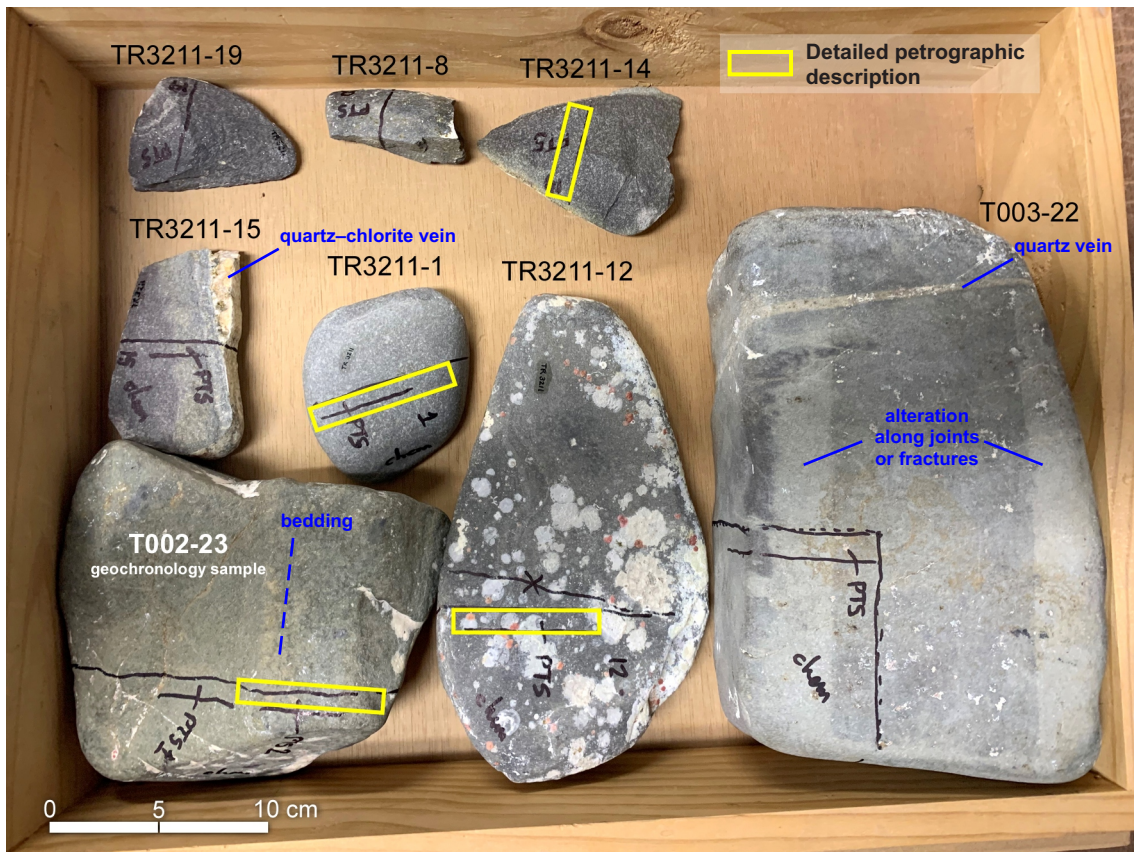
Figure 3. Ballast stones selected for petrographic study, including two not shown in Figure 2: T003-22 and T002-23. Yellow rectangles show the locations in four samples from which polished thin sections and detailed petrographic descriptions were obtained
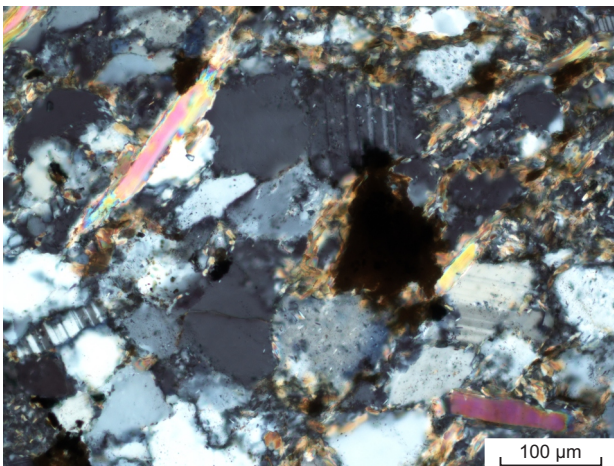
Figure 4. Photomicrograph of ballast stone sample T002-23 in cross-polarized light, showing closely packed grains of feldspar and quartz, detrital muscovite laths, and an opaque grain (ilmenite altered to non-reflective iron oxide minerals). Interstitial fine-grained biotite is interpreted as mainly detrital, although possibly redistributed during diagenesis

Figure 5. Transmitted-light image of representative zircons from sandstone sample T002-23, showing anhedral to euhedral shapes and surface pitting of some crystals

Table 1.   Summary of the petrographic characteristics of four ballast stones

Sample	Rock type	Average grain size (mm)	Quartz and feldspar shape	Sorting	Quartz	Feldspar	Biotite and muscovite	Opaque minerals	Trace minerals	Other minerals	Comment
TR3211-1	arkosic sandstone component	0.15 – 0.20, micas to 0.5	angular to sub-angular	poor	40–45%	15–20%, mainly plagioclase	35–40%, mostly biotite	2–3% ilmenite	zircon	secondary chlorite	matrix-rich; may be weakly deformed; micas interpreted as detrital
	siltstone component	<0.05, micas to 0.4	angular	–	minor	minor	major, mostly biotite	magnetite	–	secondary chlorite	siltstone also forms intraclasts in sandstone; micas interpreted as detrital
TR3211-12	siltstone	0.03 – 0.04, micas to 0.25	angular to sub-angular	–	25–30%?	20–25%?	45–50%, mostly biotite	ilmenite	tourmaline zircon	–	rock is compacted; biotite interpreted as detrital
TR3211-14	arkosic sandstone	0.25	angular to sub-angular	moderate	45%	40%, mainly plagioclase	<10%, mostly biotite	1–2% ilmenite	tourmaline zircon	3–4% chert & lithic grains	matrix-poor; weakly deformed; biotite interpreted as mainly detrital
T002-23*	arkosic sandstone	0.15, micas to 0.4	angular to sub-angular	moderate	35–40%	45–50%	7–10% biotite, 1–2% muscovite	4–5% ilmenite, mainly in HM layers	tourmaline zircon	secondary chlorite & sericite	matrix-poor; weakly deformed; micas interpreted as mainly detrital

* Geochronology sample; HM, heavy mineral

The youngest zircon (Fig. 8) indicates a 207-corrected $^{238}U/^{206}Pb*$ date of 549 ± 5 Ma (1σ), tentatively interpreted as a maximum age for sediment deposition. A more conservative estimate of the maximum depositional age can be based on the weighted mean 207-corrected $^{238}U/^{206}Pb*$ date of 580 ± 5 Ma (95% uncertainty, MSWD = 1.2) for the youngest coherent group of seven analyses (Fig. 8). Mixture modelling indicates significant age components at c. 2652, 2145, 1929, 1446, 996, 886, 795, 650 and 582 Ma, based on contributions from approximately 10, 3, 10, 4, 22, 10, 5, 28 and 10 analyses, respectively (Fig. 9).

Geochemistry

Five samples selected for whole-rock geochemistry yielded very similar results (Appendix 4). All samples are moderately to strongly peraluminous, with aluminium saturation indices (ASI = mol ratio of Al/Ca+Na+K) between 1.15 and 1.83, typical of clay-bearing sedimentary rocks, which commonly contain concentrations of aluminium in excess of that required to account for Na, K and Ca housed in feldspar. The samples show a relatively wide variation in silica, from 61.0 to 76.4 wt%, together with systematic corresponding decreases in the major element oxides Al_2O_3, Fe_2O_3, MgO and K_2O and increases in Na_2O. Mantle-normalized trace element patterns are consistent and exhibit distinctive Nb, Sr and Ti anomalies (Fig. 10).

The variations in chemistry are consistent between samples and mainly reflect physical (depositional) controls on the mineral proportions of these sedimentary rocks, and probably also reflect a sediment provenance dominated by igneous rocks – although presumably of several ages, as indicated by the detrital zircon geochronology. The consistency in results suggests the ballast stones represent a single sedimentary unit.
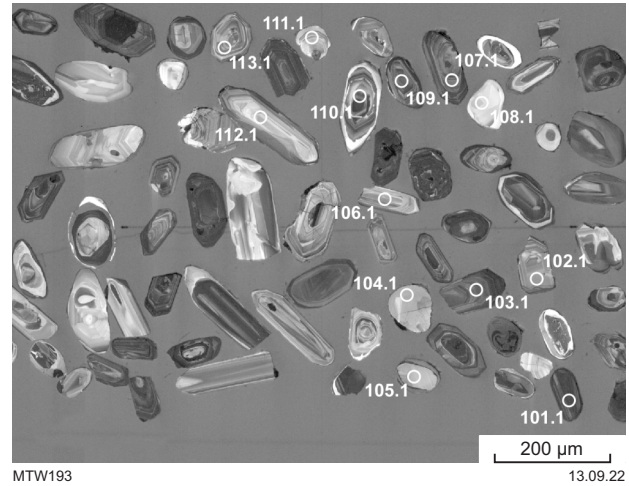
Figure 6. Cathodoluminescence (CL) image of representative zircons (same crystals shown in Figure 5) from sandstone sample T002-23, showing truncation of concentric zoning at grain boundaries in some crystals. Numbered circles indicate the approximate locations of analysis sites
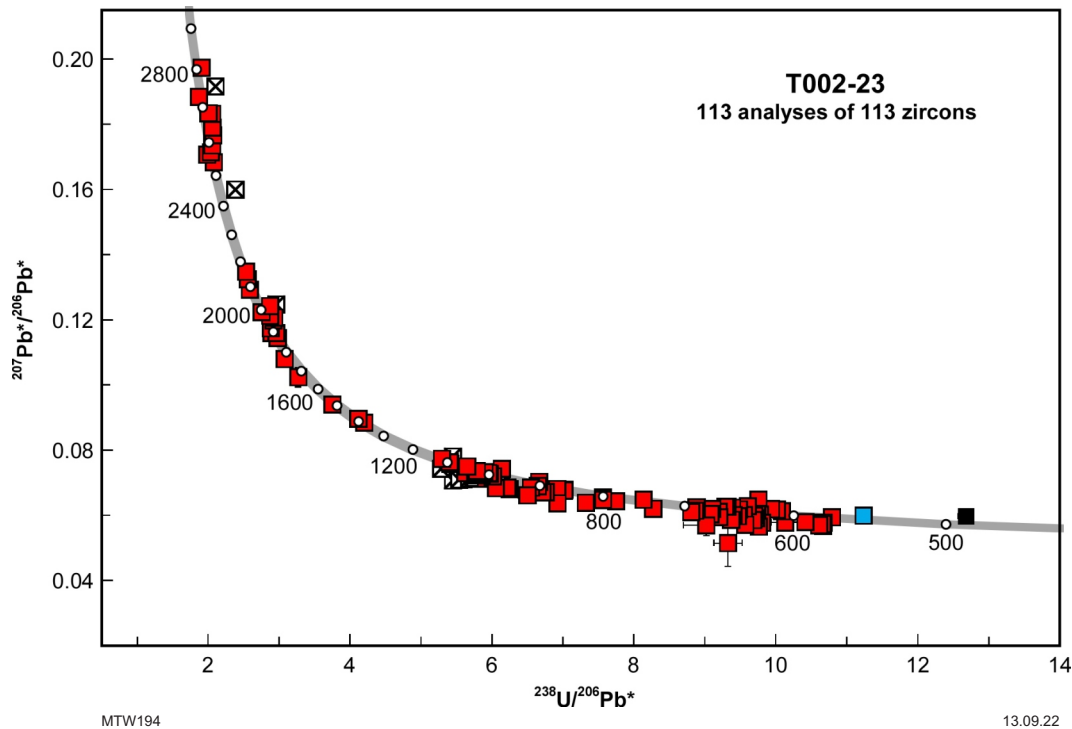
Figure 7. U–Pb analytical data, corrected for common Pb, for zircons from sandstone sample T002-23. Grey concordia curve is marked with age in millions of years (Ma). Blue square indicates the youngest detrital zircon, red squares indicate older detrital zircons, black square indicates an anomalously young result for a high-U zircon that likely reflects loss of radiogenic Pb, and crossed squares indicate analyses >1000 Ma with discordance >5%. Pb* is radiogenic Pb; error bars are ±1 sigma
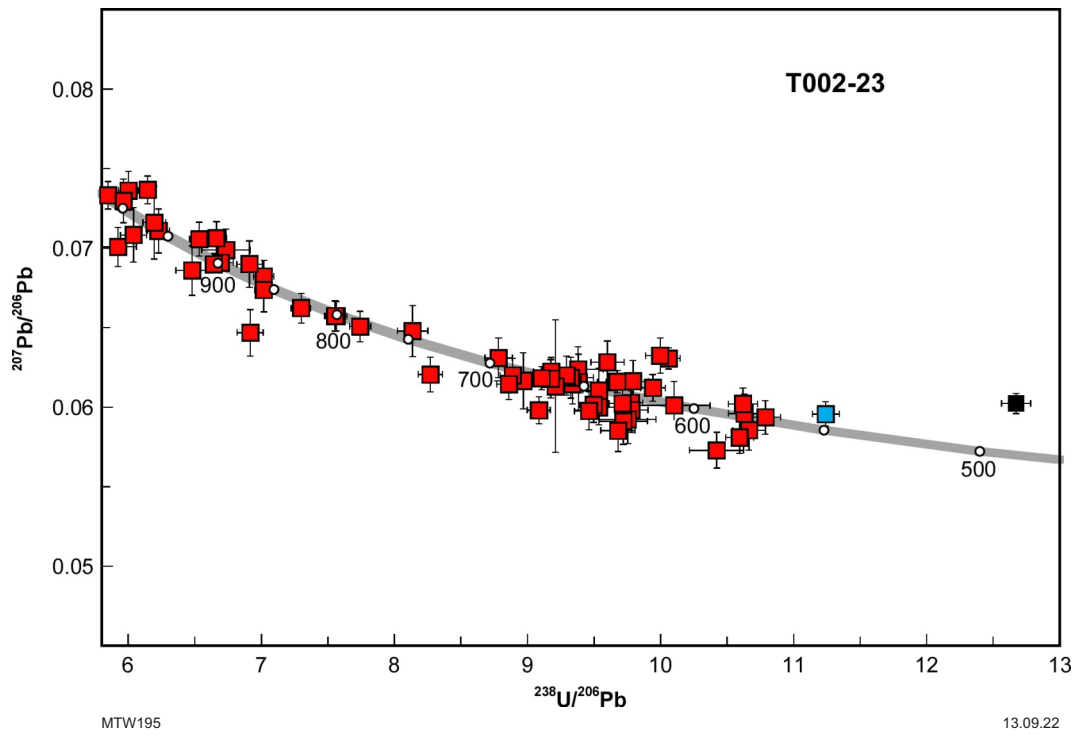
Figure 8.   Expanded view of U–Pb analytical data <1000 Ma, not corrected for common Pb, for zircons from sandstone sample T002-23. Symbols as in Figure 7
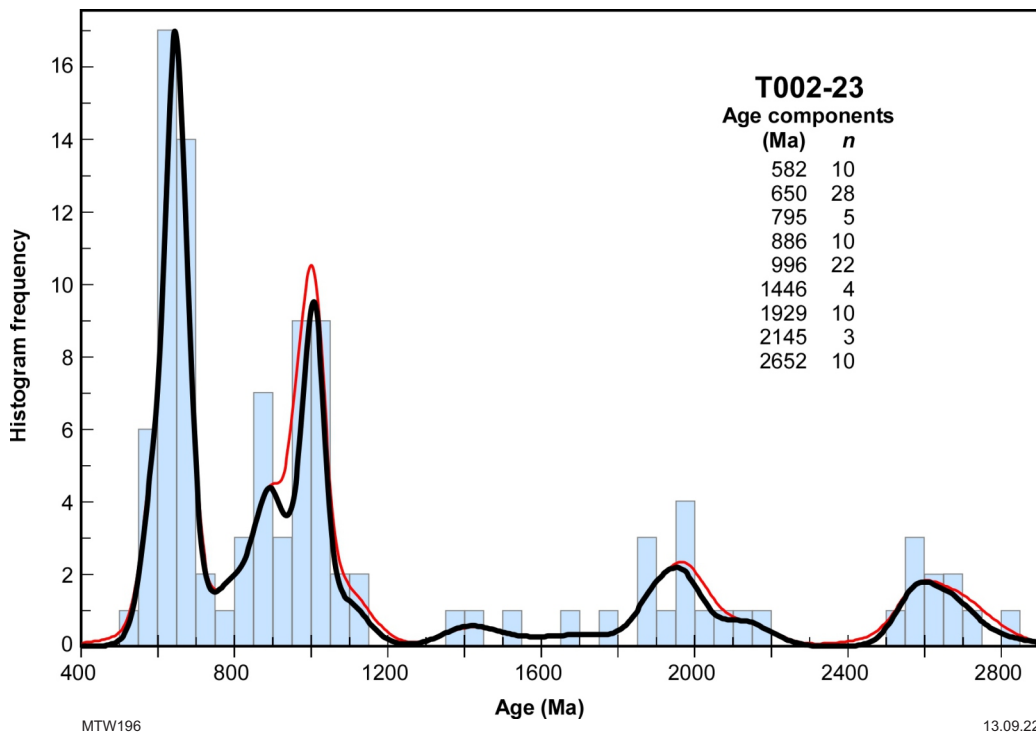
Figure 9.   Probability density (kernel density estimation) diagram and histogram of detrital zircon U–Pb ages from sandstone sample T002-23. Thick curve and histogram (bin width 50 Ma) include only accepted data (103 analyses of 103 zircons); thin curve includes all data (113 analyses of 113 zircons). Age components are estimated by maximum-likelihood mixture modelling; *n* is number of analyses
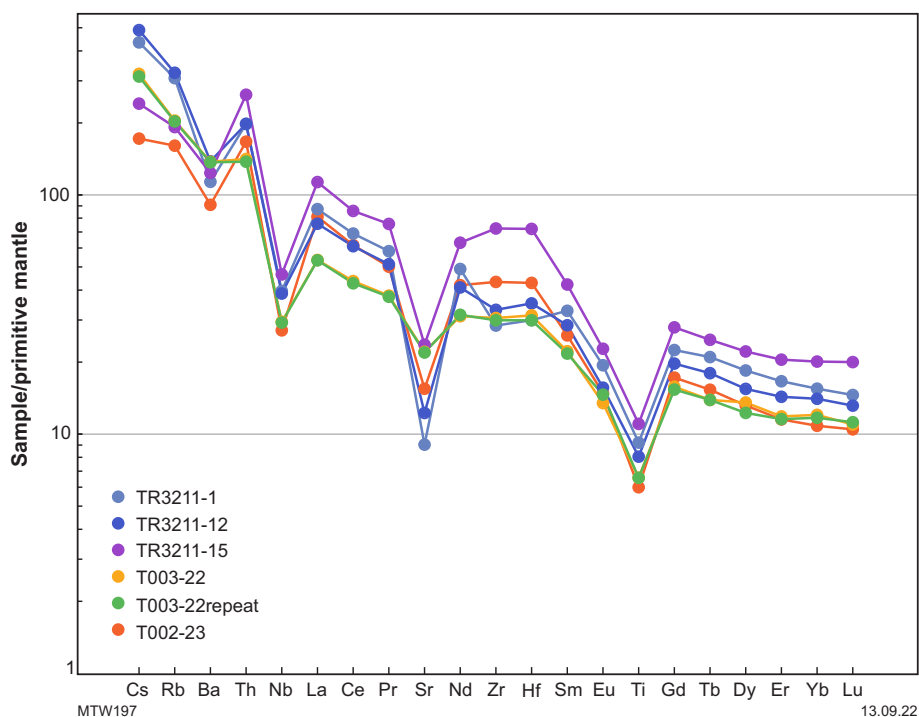
Figure 10. Trace element ratios for samples of five ballast stones (normalization to primitive mantle values after McDonough et al., 1992)

Sm–Nd isotopes

Three whole-rock samples chosen for Sm–Nd isotope analysis yield very similar results (Appendix 5), and an imprecise isochron age of c. 1.7 Ga (Fig. 11), which represents the average age of all Nd-containing components in the measured ballast stones. Two-stage depleted mantle model ages (T_{DM}^2) range from 1.83 to 1.69 Ga, with an average of c. 1.75 Ga (Fig. 11), and the consistency indicates the three samples have similar average provenance. The $^{147}Sm/^{144}Nd$ ratios are similar to that of average continental crust (0.11), so the T_{DM}^2 values are insensitive to the age chosen for calculation, and suggest that the sedimentary precursor of the ballast stones was derived from granitic sources, consistent with petrography and the abundance of detrital zircons in the studied samples. As with the geochemistry results, the consistency in isotope characteristics suggests the ballast stones represent a single sedimentary unit.

Calculated at 580 Ma (the age of the youngest detrital zircon component in ballast stone T002-23), values of $\varepsilon_{Nd(i)}$ for three ballast stones are -7.5 to -5.6. Data for sedimentary rocks of southwestern England (Darbyshire and Shepherd, 1994) are very similar although more dispersed, and indicate $\varepsilon_{Nd(i)}$ values mainly between -8.1 and -5.0 and T_{DM}^2 mainly between 1.88 and 1.64 Ga (although two outlying samples yield $\varepsilon_{Nd(i)}$ of -3 and -2 and T_{DM}^2 of 1.5 and 1.4 Ga).

Origin of the ballast stones

If the *Trial* took on ballast in Plymouth prior to its departure in 1621, one might expect the ballast stones to have originated in the area around Plymouth harbour or Plymouth Sound. It is also possible that the ballast stones were sourced from

another location and transported to Plymouth before being loaded onto the *Trial*. The following sections summarise the geology of the Plymouth area and southwestern England and compare the characteristics of the ballast stones to those of possible source rocks in that area, and to other possible sources in Europe. For reference, a geological time scale is provided in Figure 12.

Geology of Plymouth Sound and southwestern England

Southwestern England consists mainly of Devonian to Carboniferous sedimentary rocks, recognized as correlatives of the Rhenohercynian Zone of Europe and the South Portuguese Zone of Iberia (Fig. 13) (Floyd et al., 1990; Leveridge and Hartley, 2006). Collectively, these regions form a belt of sedimentary basins that formed during the Variscan Orogeny, and represent a passive margin sequence developed during Devonian to Carboniferous extension of the southern edge of the Avalonia Terrane that was accreted to Laurussia (Laurentia + Baltica) as the Iapetus and Rheic Oceans closed during assembly of Pangea (Keppie et al., 2003; Leveridge and Hartley, 2006; Shail and Leveridge, 2009). Southwestern England was juxtaposed against rocks of unequivocal Avalonia affinity to the northeast via several hundred kilometres of dextral displacement along the Bristol Channel – Bray Fault (BCBF in Fig. 13) during the late Carboniferous.

The Paleozoic sedimentary successions of southwestern England were deposited in a series of east–west-trending graben and half-graben (Fig. 14) that developed sequentially northwards during Devonian rifting of the Rhenohercynian passive margin (Leveridge, 2011). The oldest is the Lower Devonian Looe Basin, which consists of non-marine

sedimentary rocks of the Dartmouth Group, overlain by mainly shallow-marine rocks of the Meadfoot Group, together with subordinate bimodal rift-related igneous rocks (Richter, 1967; Seago, 1991; Leveridge et al., 2002; Leveridge, 2011). Devonian fossils, including fish remains (e.g. *Pteraspis*), ammonoids, trilobites, brachiopods, conodonts and corals are relatively common in some units (Ussher, 1907).

The Dartmouth Group consists mainly of mudrock and minor sandstone deposited in a distal alluvial fan setting (Seago, 1991). Black mudrock of the Bovisand Formation of the lower Meadfoot Group records a major marine transgression, whereas the overlying Staddon Formation represents a minor regressive pulse and significant input of non-marine sediment from the north during the late Early Devonian (Seago, 1991; Shail and Leveridge, 2009).
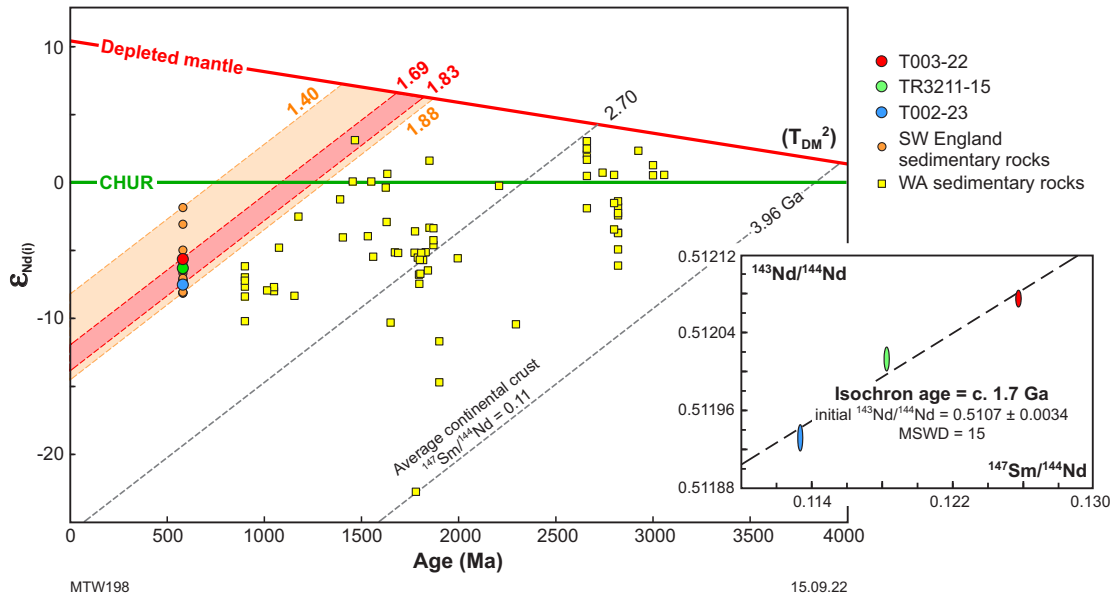
Figure 11. Samarium–neodymium (Sm–Nd) evolution diagram showing results for three ballast stone samples, together with data for sedimentary rocks in southwestern England (Darbyshire and Shepherd, 1994), all calculated and plotted at 580 Ma. Data for sedimentary rocks in Western Australia are included for comparison (Lu et al., 2022). Models of mantle reservoir evolution are CHUR (chondritic uniform reservoir, Bouvier et al., 2008) and Depleted mantle (Champion and Huston, 2016). Dashed lines indicate the Nd evolution of average continental crust (Champion and Huston, 2016). The inset shows an isochron diagram in which an imprecise regression indicates a date of c. 1.7 Ga (billion years)
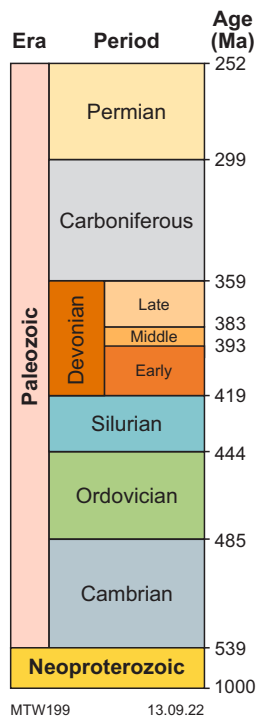
Figure 12. Simplified Neoproterozoic and Paleozoic time scale, showing approximate ages of Period boundaries in Ma (million years). Excerpted from Cohen et al. (2013, updated 2022).
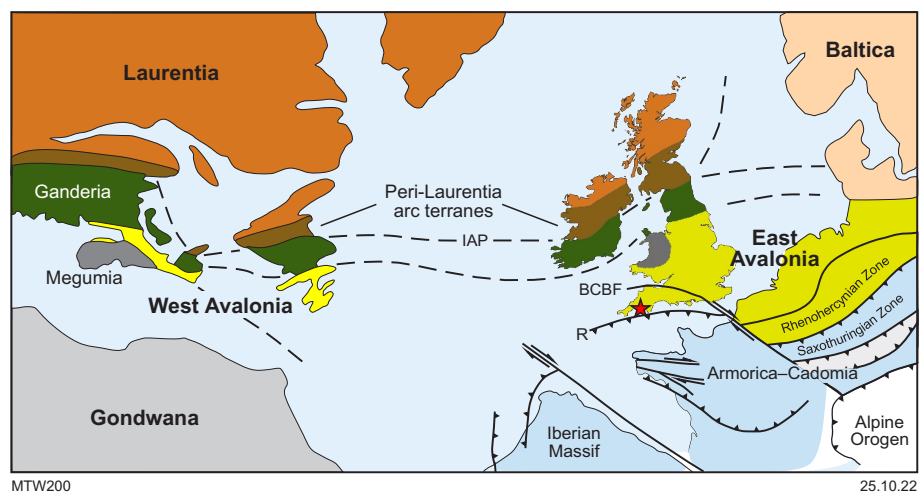
Figure 13. Tectonic setting of southwestern England following late Carboniferous closure of the Iapetus and Rheic Oceans and dextral transposition of southwestern England along the Bristol Channel – Bray Fault (BCBF) (after Leveridge and Hartley, 2006; Shail and Leveridge, 2009; Nance et al., 2010; Murphy et al., 2014). Thick black lines indicate major faults: thrust faults have teeth on the upper plate; arrows on transcurrent faults indicate directions of motion. Dashed lines indicate the approximate locations of major oceanic sutures (IAP, Iapetus suture; R, Rheic suture). The location of Plymouth is shown by a star
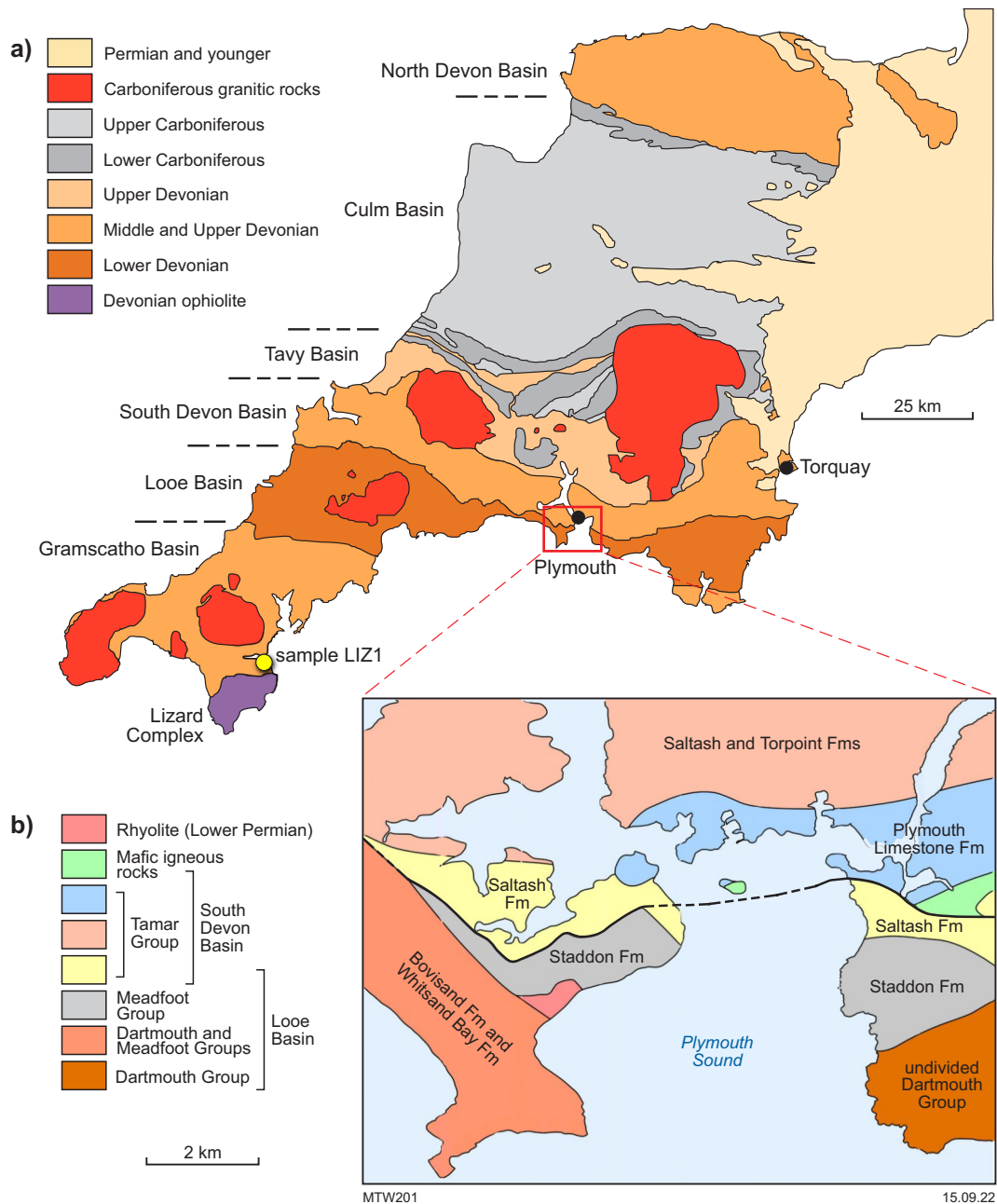
Figure 14. Regional geology of southwestern England: a) Devonian to Permian sedimentary basins, after Leveridge and Hartley (2006) and Shail and Leveridge (2009). The location of detrital zircon sample LIZ1 (Strachan et al., 2014) is shown; b) simplified geology of Plymouth Sound (after BGS, 2022)

Basin inversion and metamorphism accompanied north-directed thrusting during the Variscan Orogeny, followed by intrusion of the late Carboniferous (316–300 Ma) Cornubian granite batholith during post-orogenic extension (Alexander and Shail, 1996; Shail and Leveridge, 2009; Neace et al., 2016). Devonian deep-marine and flysch sedimentary rocks of the Gramscatho Group (Fig. 14) were thrust over rocks of the Looe Basin in the Late Devonian (Leveridge and Shail, 2011).

The metamorphic grade of Devonian rocks in the region is mostly very low, but ranges locally up to greenschist facies (Phillips, 1928; Primmer, 1985). Generally higher metamorphic grades observed in the Looe and Gramscatho Groups in the south are attributed to crustal thickening due to stacking of thrust sheets (Warr et al., 1991). Although biotite is relatively rare or absent in most rocks, biotite is locally a major constituent (Phillips, 1928). Shannon (1928) reported minor biotite in Meadfoot Group quartzites in the Plymouth area. The Baggy Sandstone, on the northern coast of Devon, contains abundant biotite and muscovite, similar to the ballast stones, although this rock is slightly younger than those in the Plymouth area, being Late Devonian to Carboniferous in age (Shannon, 1928; Whittaker and Leveridge, 2011). In some phyllitic metasedimentary rocks in contact aureoles around Carboniferous granite, biotite has replaced chlorite in porphyroblastic intergrowths with muscovite (Phillips, 1928).

Comparison between the ballast stones and rocks of southwestern England

The ballast stones are lithologically similar to fine-grained sandstone or quartzite beds in both the Dartmouth and Meadfoot Groups. However, the ballast stones contain a higher proportion of biotite (Table 1) than has been described for similar rocks in the Plymouth area.

The detrital zircon age spectrum for the ballast stone sample is dominated by Neoproterozoic ages (Fig. 15i), including significant age components at c. 1000, 890, 650, and 580 Ma. The 650 and 580 Ma components are similar to results compiled for Avalonia and other peri-Gondwanan terranes that rifted away from Gondwana in the Neoproterozoic and then were progressively accreted to Laurussia during the Paleozoic (Fig. 15c–g; e.g. Nance et al., 2010). Minor age components at c. 2650, 2150, 1930 and 1450 Ma are also consistent with a peri-Gondwanan provenance. However, the c. 1000 and 890 Ma age components that are so significant in the ballast stone sample are not prominent in the compiled age spectra for peri-Gondwanan terranes (although there are numerous rocks of this age in the Armorica–Cadomia belt of Europe, e.g. Murphy et al., 2002, and references therein). Alternatively, these early Neoproterozoic ages could reflect derivation from Baltica and/or Laurentia (Fig. 15a,b). Note that the compiled age spectra each includes hundreds or thousands of analyses from numerous samples (Fig. 15a–g), whereas the spectrum for the ballast stone is based on a comparatively small number of analyses from a single sample; its curve would appear reasonably compatible with most of the reference curves if scaled appropriately.

Results for a Lower Devonian feldspathic sandstone of the Meneage Formation of the Gramscatho Group (sample LIZ1, Strachan et al., 2014), sampled about 75 km to the west-southwest of Plymouth (Fig. 14a), are the only detrital zircon data available for Devonian rocks of southwestern England (Fig. 15h). The data are dominated by 620–520 Ma ages, slightly younger than the 650–580 Ma ages for the ballast stone, although this difference may not be very significant based only on results for single samples. The 1000–890 Ma ages for the ballast stone are not represented in the Gramscatho Group sample (one analysis at 1035 Ma), although the older c. 2.6 and 2.0 Ga ages are similar.

At c. 580 Ma, the youngest detrital zircon age component in ballast stone sample T002-23 is about 160 Ma older than the accepted Early Devonian (419–383 Ma) depositional age of the Dartmouth and Meadfoot Group samples (Fig. 15i). Similarly, the youngest age component in the Gramscatho Group sample is >100 Ma older than its inferred depositional age (Fig. 15h). However, these apparent age gaps are to be expected in passive margin extensional basins where high-relief sediment sources are absent (Cawood et al., 2012).
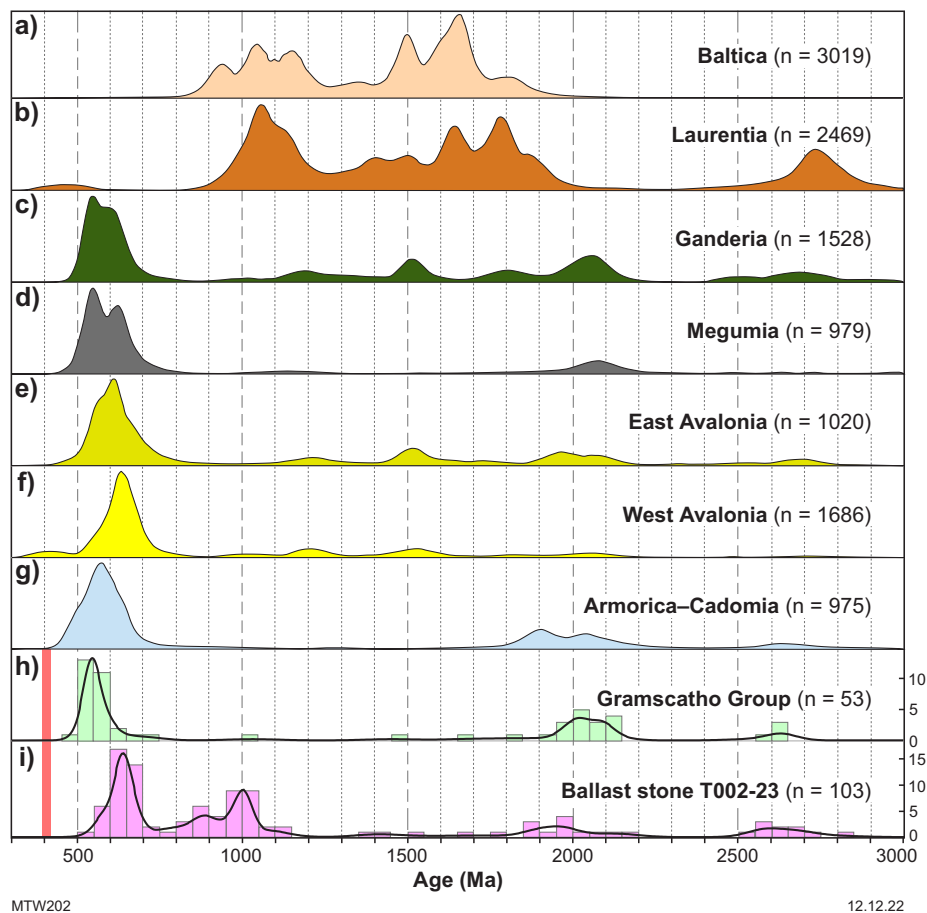
Figure 15. Detrital zircon age spectra for potential source terranes (a–g) and a Gramscatho Group sample (h) compared with data for ballast stone T002-23 (i). Colours in (a) to (g) correspond to those of terranes in Figure 13. Compilations are from (a) Stephan et al., (2019), (b–g) Stevens and Baykal (2021), and references within, and data in (h) are from Strachan et al. (2014). *n* = number of individual zircon dates. In (h) and (i), vertical scales indicate histogram frequency and the vertical red bar indicates the approximate depositional age of Lower Devonian rocks in southwestern England

The Nd isotope characteristics of three ballast stones are an excellent match with those of Paleozoic sedimentary rocks in southwestern England (Darbyshire and Shepherd, 1994), including the Meadfoot Group exposed in Plymouth Sound (Fig. 11). In both cases, values of ε_{Nd} are -8 to -5 and model ages ($T_{DM}{}^2$) are between 1.9 and 1.6 Ga, averaging about 1.7 Ga. Nd isotope compositions for both the ballast stones and sedimentary rocks of southwestern England are also distinct from, and more radiogenic than, most sedimentary rocks in Western Australia (Lu et al., 2022), although relatively few sedimentary samples in Western Australia have been measured.

The characteristics of the ballast stones are broadly consistent with an origin in southwestern England, including Plymouth. However, although biotite-rich sandstone has been described from the region, the high content of biotite in the ballast stones is not typical of most rocks in the Plymouth area.

Other possible sources

Outside southwestern England, there are few localities in Britain where the ballast stones could have originated. A simplified geological map of Britain is shown in Figure 16a, and a map showing only rocks of suitable age (Neoproterozoic to Devonian) is shown in Figure 16b. Rocks in this age range are common in Wales, whereas most sedimentary rocks elsewhere in England are Mesozoic or younger (i.e. <252 Ma), and could not have been the source of the ballast stones.

There are Neoproterozoic and Paleozoic rocks in the Armorican, Iberian and Bohemian massifs of Europe that may be similar to the ballast stones (e.g. Murphy et al., 2002, and references therein), although many are located in inland areas away from ocean or harbour settings. A detailed assessment of these possibilities is beyond the scope of this study. The Armorican massif of northwestern France includes Neoproterozoic and Paleozoic rocks (e.g. Vidal et al., 2011), together with suitable harbours, such as Brest, although that port did not engage in shipbuilding in the early 1600s (Britannica, 2017). The northwestern Iberian peninsula features numerous Proterozoic and Paleozoic rock units, and those adjacent to the Portuguese shipbuilding city of Porto, for example, are potential sources of the ballast stones. Although many ships that crossed the Indian Ocean towards Australia in the 17th century were Dutch, there are no rocks in the Netherlands that are similar to the ballast stones, and those ships typically carried clay bricks as ballast (Green, 1977).

Conclusions

The ballast stones consist of siltstone and fine-grained feldspathic sandstone, and strong rounding of several stones indicates they were collected from a river or ocean beach setting. Angular grain shapes and the presence of detrital feldspars and micas suggest the sediments were sourced mainly from granitic rocks and underwent limited sedimentary transport. Some stones are weakly deformed and all are rich in biotite.

Sediment deposition was younger than c. 580 Ma, based on U–Pb geochronology of detrital zircons in one ballast stone sample, and the age spectrum is dominated by Neoproterozoic components at c. 580, 650, 890, and 1000 Ma, and minor older components between c. 1400 and 2800 Ma. The wide range of detrital zircon ages implies sediment derivation from sources of different ages, or from reworking of precursor sediments that contained zircons from such sources. The zircons range from euhedral and faceted to anhedral and strongly rounded, also suggesting a mixture of proximal and distal sources. Geochemistry indicates moderately to strongly peraluminous compositions, with relatively large variations in silica and distinctive Nb, Sr and Ti anomalies. This suggests a sedimentary provenance dominated by igneous rocks. The consistency in composition is consistent with derivation of the samples from a single sedimentary unit. Sm–Nd isotopes in three stones are also very consistent, and indicate $\varepsilon_{Nd(i)}$ values of -7.5 to -5.6 (calculated at 580 Ma), and an imprecise isochron age of c. 1.7 Ga.

The ballast stones are lithologically similar to Lower to Middle Devonian sandstone and siltstone of the Dartmouth and Meadfoot Groups exposed in Plymouth Sound and elsewhere in southwestern England. Although the high biotite content of the ballast stones is unusual in sandstones of southwestern England, similar examples have been described in the literature, hence this characteristic may not be sufficient to exclude the area from consideration. The Sm–Nd isotope results in particular are an excellent match with limited data for Paleozoic sedimentary rocks of southwestern England, including the Meadfoot Group. The dominant Neoproterozoic and minor older detrital zircon age components observed for one ballast stone are typical of peri-Gondwana terranes, such as Avalonia and the Armorica–Cadomia belt of Europe.

Most other rocks in Britain that could have been sources of the ballast stones are not located close to a port engaged in shipbuilding in the early 1600s, hence Plymouth remains the most likely origin in Britain. Based on the results of this study, an origin for the ballast stones in Plymouth Sound or the surrounding area cannot be ruled out. However, several localities in Europe are also possible sources of the ballast stones, for example Porto, which has a long shipbuilding history.
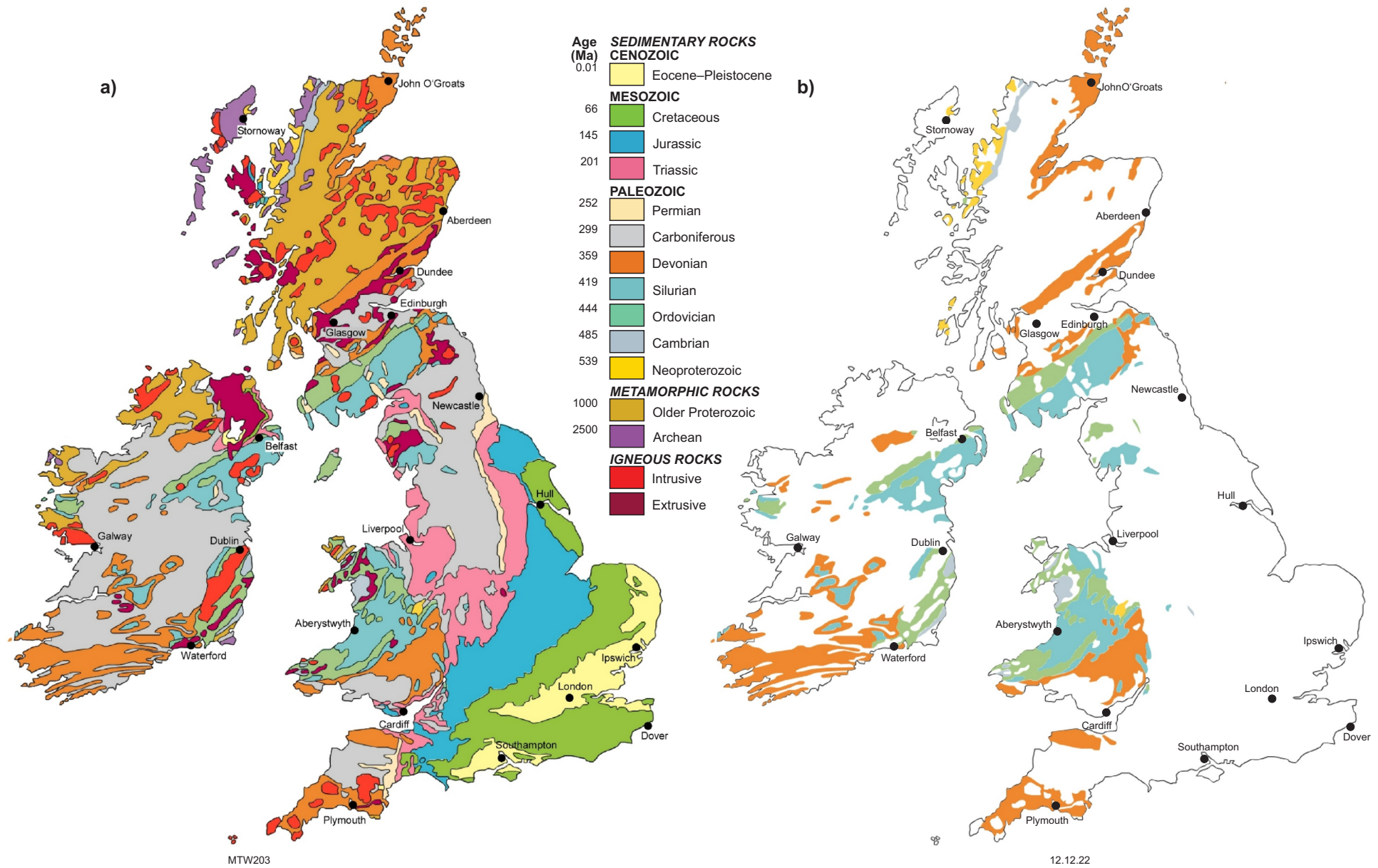
Figure 16. Simplified geology of Great Britain and Ireland: a) rocks in most of England, apart from those in Wales, are mostly Mesozoic and younger; b) Neoproterozoic to mid-Paleozoic rocks that are of suitable age to possibly have been the source of ballast stones recovered from the wreck site. Maps are modified from BGS (2022)

References

Alexander, AC and Shail, RK 1996, Late- to post-Variscan structures on the coast between Penzance and Pentewan, south Cornwall: Proceedings of the Ussher Society, v. 9, p. 72–78.

BGS (British Geological Survey) 2022, Maps: discovering geology – maps and resources: British Geological Survey online resource, viewed 5 March 2022, <www.bgs.ac.uk/discovering-geology/maps-and-resources/maps/>.

Bouvier, A, Vervoort, JD and Patchett, PJ 2008, The Lu–Hf and Sm–Nd isotopic composition of CHUR: constraints from unequilibrated chondrites and implications for the bulk composition of terrestrial planets: Earth and Planetary Science Letters, v. 273, no. 1–2, p. 48–57.

Britannica (Encyclopaedia Britannica) 2017, Brest, viewed 4 September 2022, <www.britannica.com/place/Brest-France>.

Cawood, PA, Hawkesworth, CJ and Dhuime, B 2012, Detrital zircon record and tectonic setting: Geology, v. 40, p. 875–878.

Champion, DC and Huston, DL 2016, Radiogenic isotopes, ore deposits and metallogenic terranes: Novel approaches based on regional isotopic maps and the mineral systems concept: Ore Geology Reviews, v. 76, p. 229–256.

Cohen, KM, Finney, SC, Gibbard, PL and Fan, JX 2013; updated February 2022, The ICS International Chronostratigraphic Chart: Episodes, v. 36, p. 199–204.

Darbyshire, DPF and Shepherd, TJ 1994, Nd and Sr isotope constraints on the origin of the Cornubian batholith, SW England: Journal of the Geological Society, v. 151, p. 795–802.

Floyd, PA, Leveridge, BE, Franke, W, Shail, R and Dörr, W 1990, Provenance and depositional environment of Rhenohercynian synorogenic greywackes from the Giessen Nappe, Germany: Geologische Rundschau, v. 79, p. 611–626.

Green, JN 1977, Australia's oldest wreck: the historical background and archaeological analysis of the wreck of the English East India Company's ship *Trial*, lost off the coast of Western Australia in 1622: British Archaeological Reports, Supplementary Series 27, Oxford, 57p.

Keppie, JD, Nance, RD, Murphy, JB and Dostal, J 2003, Tethyan, Mediterranean, and Pacific analogues for the Neoproterozoic–Paleozoic birth and development of peri-Gondwanan terranes and their transfer to Laurentia and Laurussia: Tectonophysics, v. 365, p. 195–219.

Leveridge, BE 2011, The Looe, South Devon and Tavy Basins: The Devonian rifted passive margin successions: Proceedings of the Geologists' Association, v. 122, p. 616–717.

Leveridge, BE and Hartley, AJ 2006, The Variscan Orogeny: the development and deformation of Devonian/Carboniferous basins in SW England and South Wales, *in* The geology of England and Wales, *edited by* PJ Brenchley and PF Rawson: Geological Society, London, UK, p. 225–255.

Leveridge, BE, Holder, MT, Goode, AJJ, Scrivener, RC, Jones, NS and Merriman, RJ 2002, Geology of the Plymouth and south-east Cornwall area: Memoir of the British Geological Survey, sheet 348 (England and Wales), 157p.

Leveridge, BE and Shail, RK 2011, The Gramscatho Basin, south Cornwall, UK: Devonian active margin successions: Proceedings of the Geologists' Association, v. 122, p. 568–615.

Lu, Y, Wingate, MTD, Champion, DC, Smithies, RH, Johnson, SP, Gessner, K, Mole, D, Poujol, M, Maas, R, Zhao, J and Creaser, RA 2022, Samarium–neodymium isotope map of Western Australia: Geological Survey of Western Australia, digital data layer, <www.dmirs.wa.gov.au/geoview>.

McDonough, WF, Sun, S-S, Ringwood, AE, Jagoutz, E and Hofmann, AW 1992, K, Rb and Cs in the earth and moon and the evolution of the earth's mantle: Geochimica et Cosmochimica Acta, v. 56, p. 1001–1012.

Murphy, JB, Eguiluz, L and Zulauf, G 2002, Cadomian Orogens, peri-Gondwanan correlatives and Laurentia–Baltica connections: Tectonophysics, v. 352, p. 1–9.

Murphy, JB, Waldron, JWF, Schofield, DI, Barry, TL and Band, AR 2014, Highly depleted isotopic compositions evident in Iapetus and Rheic Ocean basalts: implications for crustal generation and preservation: International Journal of Earth Sciences, v. 103, p. 1219–1232.

Nance, RD, Gutierrez-Alonso, G, Keppie, JD, Linnemann, U, Murphy, JB, Quesada, C, Strachan, RA and Woodcock, NH 2010, Evolution of the Rheic Ocean: Gondwana Research, v. 17, p. 194–222.

Neace, ER, Nance, RD, Murphy, JB, Lancaster, PJ and Shail, RK 2016, Zircon LA-ICPMS geochronology of the Cornubian Batholith, SW England: Tectonophysics, v. 681, p. 332–352.

Phillips, FC 1928, Metamorphism in the Upper Devonian of N. Cornwall: Geological Magazine, v. 65, p. 541–556.

Primmer, TJ 1985, A transition from diagenesis to greenschist facies within a major Variscan fold/thrust complex in south-west England: Mineralogical Magazine, v. 49, p. 365–374.

Richter, D 1967, Sedimentology and facies of the Meadfoot Beds (Lower Devonian) in south-east Devon (England): Geologische Rundschau, v. 56, p. 543–561.

Seago, RD 1991, Tectonics and sedimentation in the Devonian and Carboniferous rocks of SW Devon, England: University of Plymouth, Plymouth, England, PhD thesis (unpublished).

Shail, RK and Leveridge, BE 2009, The Rhenohercynian passive margin of SW England: Development, inversion and extensional reactivation: Comptes Rendus Geoscience, v. 341, v. 140–155.

Shannon, WG 1928, Appendix on the petrography of the Devonian sedimentary rocks: Proceedings of the Geologists' Association, v. 39, p. 137–153.

Stephan, T, Kroner, U and Romer, RL 2019, The pre-orogenic detrital zircon record of the Peri-Gondwanan crust: Geological magazine, v. 156. p. 281–307.

Stevens, T and Baykal, Y 2021, Detrital zircon U–Pb ages and source of the late Palaeocene Thanet Formation, Kent, SE England: Proceedings of the Geologists' Association, v. 132, p. 240–248.

Strachan, RA, Linnemann, U, Jeffries, T, Drost, K and Ulrich, J 2014, Armorican provenance for the melange deposits below the Lizard ophiolite (Cornwall, UK): evidence for Devonian obduction of Cadomian and Lower Palaeozoic crust onto the southern margin of Avalonia: International Journal of Earth Sciences, v. 103, p. 1359–1383.

Ussher, WAE 1907, The geology of the country around Plymouth and Liskeard: Memoirs of the Geological Survey, England and Wales, Explanation of sheet 348, 156p.

Vidal, M, Davard, M-P, Gourvennec, R, Le Hérissé, A, Loi, A, Paris, F, Plusquellec, Y and Racheboeuf, PR 2011, Le Paléozoïque de la presqu'île de Crozon, Massif armoricain (France): Géologie de la France, v. 1, p. 3–45.

Warr, LN, Primmer, TJ and Robinson, D 1991, Variscan very low-grade metamorphism in southwest England: a diasthathermal and thrust-related origin: Journal of Metamorphic Geology, v. 9, p. 751–764.

Whittaker, A and Leveridge, BE 2011, The North Devon Basin: a Devonian passive margin shelf succession: Proceedings of the Geologists' Association, v. 122, p. 718–744.

Appendix 1.

Detailed petrographic descriptions

Sandstone T002-23 (geochronology sample)

This sample is a fine-grained arkosic sandstone, consisting of about 45–50% feldspar, 35–40% quartz, 7–10% biotite, 4–5% opaque minerals (mostly ilmenite), 1–2% muscovite and accessory tourmaline and zircon. The average grain size is about 0.15 mm. The sandstone contains two discontinuous bands up to 0.3 mm wide of concentrations of iron oxide minerals, mostly ilmenite and leucoxene, as well as zircon and tourmaline (Fig. A1).
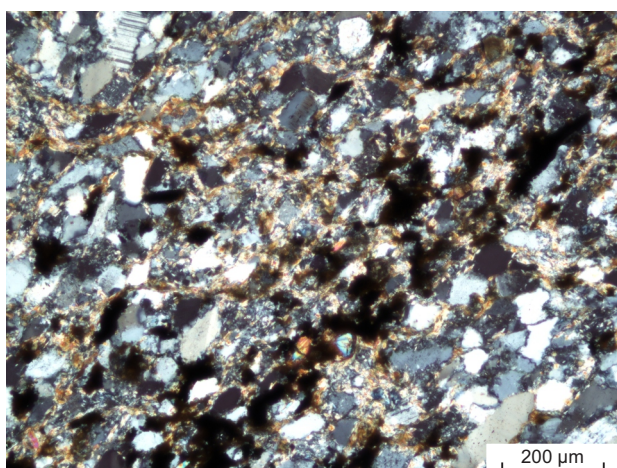
MTW204   13.09.22

Figure A1. Photomicrograph of sample T002-23 in cross-polarized light of a narrow heavy mineral layer (on diagonal) within fine-grained sandstone composed mainly of feldspar and quartz. The heavy mineral layer is mainly ilmenite (opaque) but also includes zircons (e.g. two bright high-relief grains below centre). Fine-grained biotite grains around quartz and feldspar are interpreted as detrital, although some may have been redistributed during diagenesis

Feldspars are angular to sub-angular, equant to elongate, and mostly <0.2 mm in size, although some are up to 0.3 mm. Some feldspars that are finely altered to clay minerals and sericite and/or exhibit fine multiple twinning are probably plagioclase. Less-altered non-twinned grains are probably alkali feldspar. Quartz forms mainly sub-angular, equant and less abundant elongate grains, which range in size up to 0.2 mm, with an average grain size of 0.15 mm. Quartz is transparent and either unstrained or weakly strained. Biotite with minor sericite and trace chlorite occurs in very fine-grained aggregates that surround detrital grains and form narrow discontinuous folia (Fig. A2). The aggregates are interpreted as detrital grains redistributed along grain boundaries by circulation of diagenetic fluid. Trace well-formed biotite laths up to 0.2 mm long, and more abundant slender muscovite laths up to 0.4 mm long, are clearly detrital in origin. Muscovite laths are crudely parallel to the heavy mineral layers. Ilmenite is concentrated within the heavy mineral layers and occurs as rare, disseminated grains elsewhere in the sandstone. Ilmenite grains are up to 0.2 mm long, mostly crudely tabular, and have a very finely skeletal texture. Opaque material between the skeletal ilmenite is non-reflective and of unknown composition. Disseminated olive-green tourmaline occurs as sub-angular

and sub-rounded grains up to 0.1 mm in size. Colourless and pale pink sub-angular zircons up to 0.1 mm long are mostly concentrated in the heavy mineral layers.

Where micas are less abundant, detrital feldspar and quartz grains form a relatively closely packed aggregate. It is difficult to assess how much matrix the sandstone contains but it appears to be low. Although grains are not well rounded, the sandstone is moderately sorted, and could be classified as texturally mature. The provenance is most likely to be granitic. The sandstone has been very mildly deformed, resulting in a poorly developed anastomosing fracture cleavage at a high angle to the heavy mineral layers. Deformation has been too weak to cause strain in quartz or rotation of detrital micas into parallelism and there is no evidence of metamorphism.
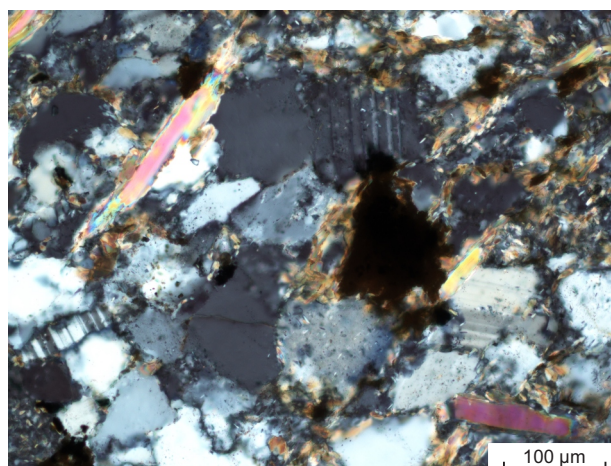
MTW205   13.09.22

Figure A2. Photomicrograph of sample T002-23 in cross-polarized light showing more detail of the sandstone texture, including closely packed grains of feldspar and quartz, large detrital muscovite laths, interstitial fine-grained biotite, and an opaque grain (ilmenite altered to non-reflective iron oxide minerals)

Sandstone and siltstone TR3211-1

The sample is a bedded sedimentary rock, and the thin section consists of about 60% sandstone and 40% siltstone, separated by a sharp and almost planar contact (Fig. A3). Aligned, highly elongate siltstone lenses up to 4 mm long occur within the sandstone are interpreted to be siltstone intraclasts.

Excluding siltstone intraclasts, the sandstone is composed of about 40–45% quartz, 35–40% micas (mostly biotite with minor muscovite and secondary chlorite), 15–20% detrital feldspar, and 2–3% opaque minerals (mostly ilmenite with minor secondary iron oxides) and zircon. Part of the quartz and feldspar content consists of well-defined, sub-angular and angular detrital grains about 0.15 – 0.20 mm in size, which are sparsely distributed throughout a finer-grained matrix of coarse silt-size grains (Fig. A3). Larger grains of quartz are transparent and almost unstrained. Feldspar grains are mostly slightly pitted or finely speckled with clay

minerals. Many feldspars display poor to well-developed multiple twinning and are mostly plagioclase, whereas a small amount of non-twinned mottled grains is probably alkali feldspar.

MTW206   13.09.22
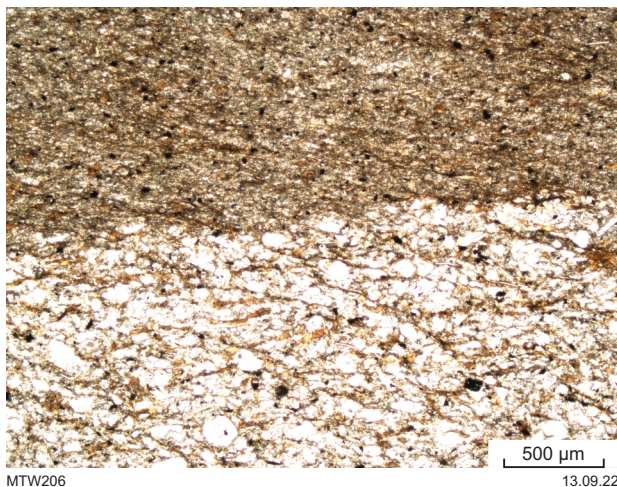
Figure A3. Photomicrograph of sample TR3211-1 in plane-polarized light showing the boundary between biotite-rich siltstone (top) and very fine-grained sandstone (bottom). A weak tectonic fabric at a low angle to bedding is evident in both lithologies

The silt-size matrix (average size <0.05 mm) consists of poorly defined, angular grains of quartz, less abundant feldspar and abundant biotite. Biotite is golden brown and forms mainly small laths up to 0.15 mm long, although some are up to 0.5 mm long. There is also a small but conspicuous amount of muscovite laths, also up to 0.5 mm in length, some of which are intergrown with biotite. Minor chlorite has replaced some of the muscovite and biotite. The relatively well-formed elongate lath shapes of biotite and much less abundant muscovite suggests these micas are detrital in origin (Fig. A4). Opaque grains are mostly ilmenite, forming disseminated, slightly irregular or skeletal grains up to 0.1 mm in diameter. Some have been replaced by secondary iron oxide minerals such as goethite and/or leucoxene. Zircon crystals (Fig. A5) are euhedral and non-abraded, up to 0.1 mm long, and it is likely that rare, tiny (10–15 µm) tabular grains in biotite are zircon or monazite.

MTW207   13.09.22
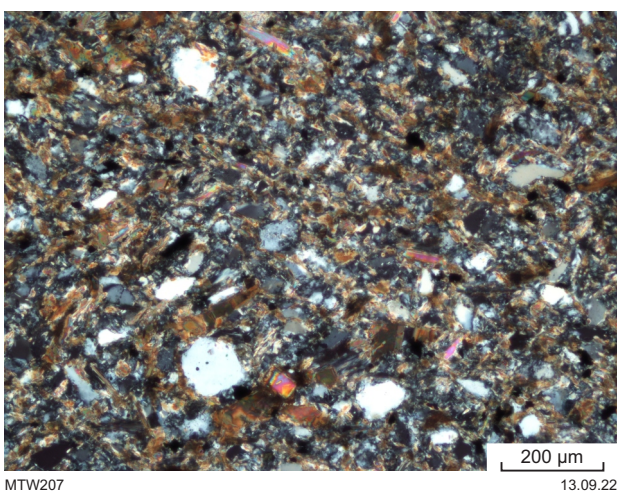
Figure A4. Photomicrograph of sample TR3211-1 in cross-polarized light showing the massive texture and biotite-rich composition of the sandstone, in which scattered larger quartz and feldspar (grey) grains occur within a silt-size aggregate of quartz, feldspar, abundant biotite and minor muscovite

MTW208   13.09.22
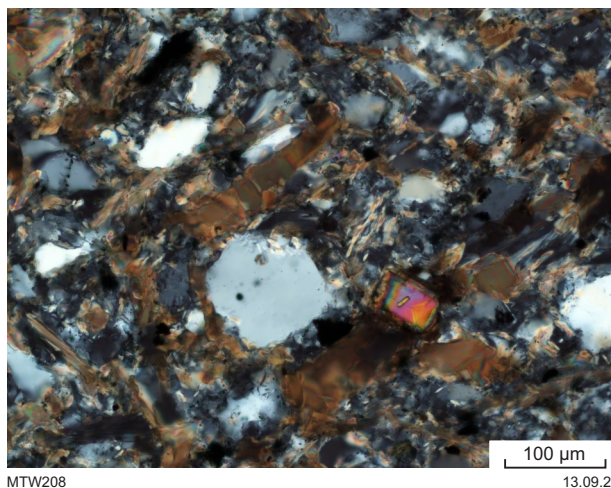
Figure A5. Photomicrograph of sample TR3211-1 in cross-polarized light of the lower part of Figure A4, showing detrital quartz and grey feldspar grains. Abundant biotite laths are interpreted as detrital, and some are slightly altered to sericite and chlorite. The birefringent grain to the right of the largest quartz grain is zircon

The siltstone layer and siltstone intraclasts consist mainly of pale to golden brown biotite and minor muscovite and chlorite, which form variably weakly aligned, ragged laths and decussate mosaics. A few larger, lozenge-shaped elongate grains of chlorite and minor biotite are up to 0.4 mm long and mostly aligned parallel to bedding. Angular grains of quartz and possible feldspar within the mica aggregate are up to 0.05 mm in size. Equant and slightly skeletal magnetite grains up to 0.05 mm in diameter are disseminated throughout the siltstone.

The sandstone has undergone compaction and mild quartz dissolution, which has resulted in partial alignment of detrital micas and very slight suturing of quartz grain boundaries. A weak preferred alignment of micas to form a discontinuous penetrative fabric at about 20° to bedding (Fig. A3), particularly within the siltstone adjacent to the sandstone contact, suggests mild deformation, although there is no evidence of metamorphism. The sandstone is very fine-grained and biotite-rich, and can be classified as a poorly sorted, matrix-rich, texturally immature greywacke. The provenance is most likely granitic.

Siltstone TR3211-12

The sample is a massive, biotite-rich coarse siltstone, with an average grain size of 0.03 – 0.04 mm. The siltstone is not bedded and is compositionally homogeneous, consisting of subequal amounts of quartz+feldspar and micas (Fig. A6). Although precise mineral proportions cannot be estimated accurately due to the small grain size, quartz content far exceeds that of confidently identifiable feldspar, and biotite is the dominant mica. Finely disseminated ilmenite, rare tourmaline, and zircon are accessory phases, and comprise 1–2% of the rock. Quartz grains are transparent, unstrained, and up to 0.1 mm in size, although most are <0.05 mm. Some quartz grains are obviously compacted and slightly elongate, but original grain shapes are mostly sub-angular and angular. Due to the small size and abundance of micas, feldspar is only recognized where it is finely twinned plagioclase (e.g. Fig. A7) and therefore may be more abundant than is apparent.

Biotite is pale to golden brown and forms aligned laths up to 0.15 mm long and minor smaller equant grains. Less abundant slender laths of muscovite are well-formed, strongly aligned and 0.10 – 0.25 mm long (Fig. A6). Ilmenite grains up to 0.07 mm in size have equant, rod-like or more irregular and skeletal shapes and are evenly disseminated throughout the siltstone. Rare olive- green tourmaline forms sub-angular equant and elongate grains up to 0.05 mm in size.

The siltstone has been compacted to produce a weak fissility but lacks a penetrative tectonic fabric. There is no evidence of recrystallization and the abundant biotite in the rock is interpreted as detrital rather than metamorphic.

MTW209   100 µm   13.09.22
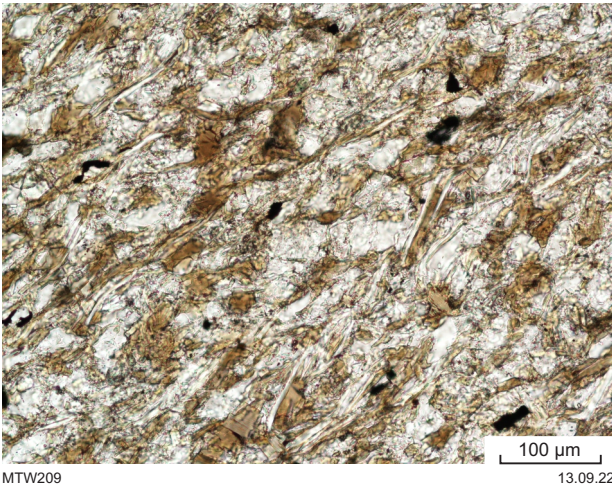
Figure A6. Photomicrograph of siltstone sample TR3211-12 in plane-polarized light showing abundant aligned laths of brown biotite and slender laths of colourless muscovite. The pale areas are mainly quartz grains

MTW210   100 µm   13.09.22
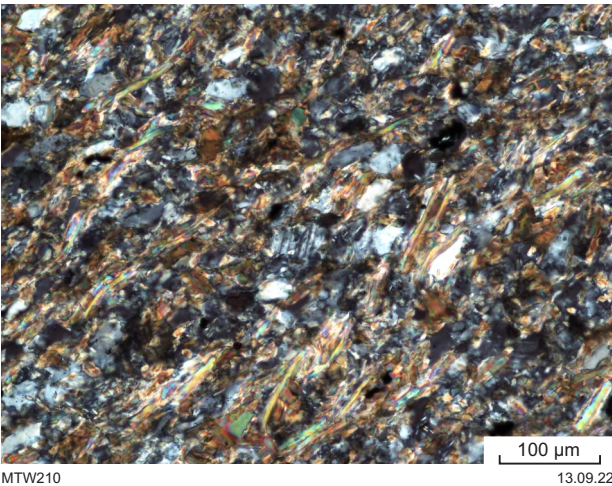
Figure A7. Photomicrograph of siltstone sample TR3211-12 in cross-polarized light, showing the same view as in Figure A6. The grain at the centre is twinned plagioclase; most of the other grey grains are quartz

Sandstone TR3211-14

This sample is a massive, medium-grained arkosic sandstone, consisting of about 45% quartz, 40% feldspar, 3–4% chert and microcrystalline quartz lithic grains, <10% biotite, 1–2% ilmenite, and accessory detrital muscovite, tourmaline and zircon (Fig. A8). The sample has a uniform average grain size of about 0.25 mm and lacks bedding or lamination.

Quartz is transparent, weakly undulose (strained), equant and slightly elongate, and up to 0.4 mm in diameter. Many grains have finely sutured boundaries with adjacent grains or with fine-grained biotite between grains, although original grain shapes are inferred to be angular and sub-angular. Detrital feldspar includes variably twinned plagioclase and subordinate microperthitic alkali feldspar. Some plagioclase has been finely sericitized. Feldspar grains are mainly equant to tabular, angular, and mostly less than 0.5 mm in size, although some isolated grains are up to 0.85 mm long. Dispersed, sub-rounded lithic grains are up to 0.25 mm in diameter and include very fine-grained massive chert and subordinate polycrystalline quartz. Laths of biotite up to 0.05 mm long form decussate aggregates, some of which form narrow selvages around other grains (Fig. A9), particularly feldspars. These may represent detrital grains redistributed along grain boundaries by circulating diagenetic fluid, although it is possible some could be hydrothermal or metamorphic in origin. Detrital muscovite forms randomly oriented, slender laths up to 0.3 mm long. Disseminated ilmenite forms equant and irregular to skeletal grains up to 0.2 mm in diameter. Blue–green tourmaline forms angular and sub-angular grains up to 0.15 mm long, and pale pink and colourless zircons are mostly non-abraded and up to 0.1 mm in size.

The sandstone is a closely packed aggregate that lacks obvious matrix. It is moderately well sorted, although the grains are angular, and the sandstone is classified as mature. Provenance is interpreted as granitic. The sandstone has undergone very weak deformation which has resulted in minor strain effects but no penetrative tectonic fabric. The rock is not metamorphosed but may have undergone diagenetic alteration to produce and/or redistribute fine-grained aggregates and folia of biotite.

MTW211   200 µm   13.09.22
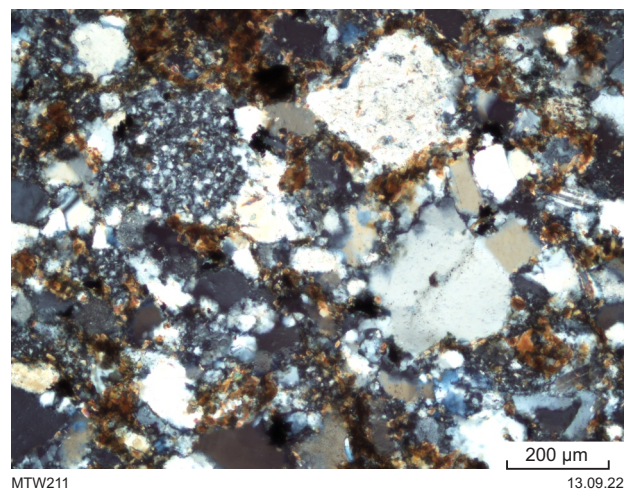
Figure A8. Photomicrograph of sample TR3211-14 in cross-polarized light, showing massive sandstone composed mainly of slightly strained quartz, speckled feldspar and very fine-grained biotite. A chert grain is visible in the upper left

MTW212   13.09.22
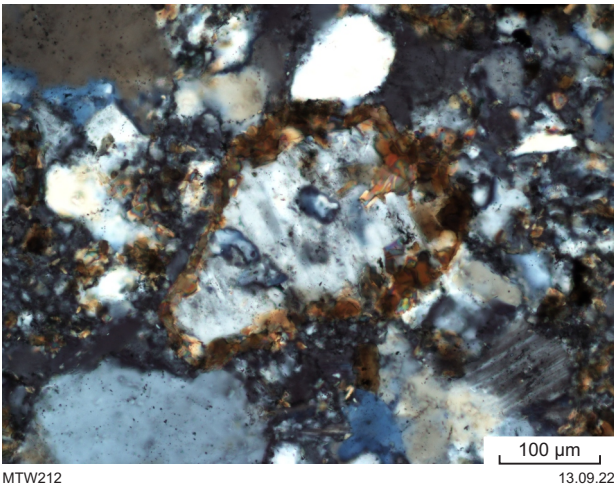
Figure A9. Photomicrograph of siltstone sample TR3211-14 in cross-polarized light, centred on a grain of alkali feldspar in the sandstone that has a mantle of secondary fine-grained biotite

Appendix 2.

Analytical methods

U–Pb geochronology

Zircons were separated using standard magnetic and density techniques, followed by hand-picking. The zircons, together with zircon reference materials, were cast in epoxy mounts and polished to expose their interiors, then characterized with transmitted light, reflected light, and cathodoluminescence (CL) images.

Zircons were analysed using the SHRIMP II ion microprobe at the John de Laeter Centre at Curtin University, Perth, using procedures detailed in Wingate et al. (2022). Analyses consisted of five scans through the mass range using a 25 μm diameter O^{2-} primary beam with an intensity of c. 2 nA. U–Th–Pb ratios and absolute abundances were determined relative to the M257 standard zircon (561.3 Ma, 840 ppm ^{238}U; Nasdala et al., 2008), analyses of which were interspersed with those of unknown zircons. Accuracy of $^{207}Pb*/^{206}Pb*$ ratios (Pb* = radiogenic Pb) was monitored during each session by analysis of the 3465 Ma OGC zircon standard (Stern et al., 2009). Data were reduced using SQUID 2.5 and Isoplot 3.71 (add-ins for Microsoft Excel; Ludwig 2003, 2009), using decay constants of Jaffey et al. (1971). Geochronology data are tabulated in Appendix 3.

During the session, 113 zircons were analysed, together with 23 analyses of the M257 standard, of which 18 analyses indicated an external spot-to-spot (reproducibility) uncertainty of 0.70% (1σ) and a $^{238}U/^{206}Pb*$ calibration uncertainty of 0.25% (1σ), both of which are included in the final uncertainties of all $^{238}U/^{206}Pb*$ ratios and dates and are listed with analytical data in Appendix 3. Isotopic mass fractionation of $^{207}Pb/^{206}Pb$ ratios during the session was corrected by reference to the OGC1 standard; measured ratios were decreased by 0.23%, equivalent to 2–3 Ma in corresponding dates.

Measured compositions were corrected for common or initial Pb using contemporaneous common Pb compositions according to the terrestrial Pb evolution model of Stacey and Kramers (1975), and either based on measured $^{204}Pb/^{206}Pb$ (204-method), or by extrapolation to concordia along a mixing line from initial Pb to yield radiogenic $^{238}U/^{206}Pb*$ ratios (207-method). Ages from analyses for which 204-corrected $^{238}U/^{206}Pb*$ ratios indicate dates <1000 Ma are based on 207-corrected $^{238}U/^{206}Pb*$ ratios; those >1000 Ma are based on 204-corrected $^{207}Pb*/^{206}Pb*$ ratios. Age components were determined using maximum-likelihood mixture modelling (Sambridge and Compston, 1994), and visualized in a probability density diagram constructed using kernel density estimation (KDE; Vermeesch, 2012).

Whole-rock geochemistry

All samples were analysed at Bureau Veritas Minerals, Canning Vale, Perth. Each sample was crushed in a plate jaw crusher and milled in a low-Cr steel mill to produce a pulp with a nominal particle size of 90% <75 μm. A representative pulp aliquot was analysed for 13 elements as major components, ignition loss, and 54 elements as trace elements (ppm). Major elements were determined by x-ray fluorescence (XRF) spectrometry on a fused glass disc. A fragment of each disc was then laser ablated and analysed by laser ablation inductively coupled plasma mass spectrometry (LA-ICP-MS) for 51 minor elements. Data are provided in Appendix 4.

Data quality was monitored by 'blind' insertion of sample duplicates (i.e. a second pulp aliquot), GSWA internal reference materials, and the certified reference material OREAS 24b (www.ore.com.au). Bureau Veritas Minerals also included duplicate samples (including OREAS 24b), variably certified reference materials, and blanks. An assessment of accuracy and precision was made using data for 17 analyses of OREAS 24b. In terms of precision, the percent relative standard deviation (RSD) or covariance for analysis of OREAS 24b is <10% for all species apart from As, Cu, Ni, Sc and Zn. Similar levels of agreement were found for parent–duplicate pairs. All blank values were less than three times the lower level of detection.

Sm–Nd isotope analysis

Sm–Nd isotope analyses were performed by isotope dilution multicollector inductively coupled plasma mass spectrometry (MC-ICPMS) at the University of Melbourne. Whole-rock sample powders (60–110 mg) were dissolved at high pressure using HF, HNO_3 and HCl at 170°C. All samples yielded clear solutions after high-pressure dissolution. Clear HCl solutions were gravimetrically split where required (high Nd concentrations) and mixed with a $^{149}Sm–^{150}Nd$ tracer. Sm and Nd were extracted following Pin and Santos-Zaldegui (1997): LREE were extracted using 0.15 ml columns of Eichrom TRU (100–150) resin, and the Sm and Nd were separated using 1 ml columns of Eichrom LN (50–100) resin. Blank corrections (<0.1 ng Sm and Nd) were negligible in all cases.

Isotope analyses were performed in static mode using a Nu Plasma MC-ICPMS (Maas et al., 2022). Data are listed in Appendix 5. Instrumental mass bias during analysis of spiked Nd and Sm fractions was corrected by internal normalization to $^{146}Nd/^{144}Nd = 0.7219$. Final $^{143}Nd/^{144}Nd$ ratios are reported relative to La Jolla Nd = 0.511860. Internal precision for $^{143}Nd/^{144}Nd$ is listed as 2 s.e. in Appendix 5. External precision for $^{143}Nd/^{144}Nd$ is ±0.000020 (2 s.d.). External precision for $^{147}Sm/^{144}Nd$ by isotope dilution is ±0.2% (2 s.d.). Results for USGS basalt standards BCR-2 and BHVO-2 and for the JNd-1 Nd isotope standard obtained in the session fall within the range of published values (Tanaka et al., 2000). The isotope calculations are based on a chondritic uniform reservoir (CHUR) model with modern-day CHUR values of $^{147}Sm/^{144}Nd = 0.1960$ and $^{143}Nd/^{144}Nd = 0.512630$ (Bouvier et al., 2008), a depleted mantle (DM) model with modern-day DM values of $^{147}Sm/^{144}Nd = 0.2136$ and $^{143}Nd/^{144}Nd = 0.513163$, and an assumed $^{147}Sm/^{144}Nd$ value of 0.11 for average continental crust (Champion and Huston, 2016).

A whole-rock Nd model age can be calculated for sedimentary rocks, although the result must be considered somewhat differently to a model age for an igneous rock.

Mixing of material (e.g. during sedimentation) from sources having different model ages is the normal situation for sedimentary rocks. In this case, the rock will produce an intermediate (mixed) result, which can be interpreted as a minimum model age for the oldest component and a maximum model age for the youngest component. In essence, this is a weighted mean model age for all Nd-containing components in the sediment (with the weighting according to the Nd concentration). Model ages in (meta)sedimentary rocks are useful for delineating provenance regions, and for discerning significant changes in provenance that may reflect unconformities within a sedimentary sequence.

References

Bouvier, A, Vervoort, JD and Patchett, PJ 2008, The Lu–Hf and Sm–Nd isotopic composition of CHUR: Constraints from unequilibrated chondrites and implications for the bulk composition of terrestrial planets: Earth and Planetary Science Letters, v. 273, no. 1–2, p. 48–57.

Champion, DC and Huston, DL 2016, Radiogenic isotopes, ore deposits and metallogenic terranes: Novel approaches based on regional isotopic maps and the mineral systems concept: Ore Geology Reviews, v. 76, p. 229–256.

Darbyshire, DPF and Shepherd, TJ 1994, Nd and Sr isotope constraints on the origin of the Cornubian batholith, SW England: Journal of the Geological Society, v. 151, p. 795–802.

Jaffey, AH, Flynn, KF, Glendenin, LE, Bentley, WC and Essling, AM 1971, Precision measurements of half-lives and specific activities of ^{235}U and ^{238}U: Physics Review C, v. 4, p. 1889–1906.

Ludwig, KR 2003, Isoplot 3.00, A geochronological toolkit for Microsoft Excel: Berkeley Geochronology Centre, Special Publication 4, 70p.

Ludwig, KR 2009, Squid 2.50, A user's manual: Berkeley Geochronology Centre, Berkeley, California, USA, 95p. (unpublished report).

Maas, R, Apukhtina, O, Kamenetsky, VS, Ehrig, K, Sprung, P and Münker, C 2022, Carbonates at the supergiant Olympic Dam Cu–U–Au–Ag deposit, South Australia, Part 2: Sm–Nd, Lu–Hf and Sr–Pb isotope constraints on the chronology of carbonate deposition: Ore Geology Reviews, v. 140, 103745, doi.org/10.1016/j.oregeorev.2020.103745.

Nasdala, L, Hofmeister, W, Norberg, N, Mattinson, JM, Corfu, F, Dörr, W, Kamo, SL, Kennedy, AK, Kronz, A, Reiners, PW, Frei, D, Kosler, J, Wan, Y, Götze, J, Häger, T, Kröner, A and Valley, JW 2008, Zircon M257 — a homogeneous natural reference material for the ion microprobe U–Pb analysis of zircon: Geostandards and Geoanalytical Research, v. 32, p. 247–265.

Pin, C and Santos-Zalduegui, JF 1997, Sequential separation of light rare-earth elements, thorium and uranium by miniaturised extraction chromatography: Application to isotopic analyses of silicate rocks: Analytica Chimica Acta, v. 339, p. 79–89.

Sambridge, MS and Compston, W 1994, Mixture modelling of multi-component data sets with application to ion-probe zircon ages: Earth and Planetary Science Letters, v. 128, p. 373–390.

Stacey, JS and Kramers, JD 1975, Approximation of terrestrial lead isotope evolution by a two-stage model: Earth and Planetary Science Letters, v. 26, p. 207–221.

Stern, RA, Bodorkos, S, Kamo, SL, Hickman, AH and Corfu, F 2009, Measurement of SIMS instrumental mass fractionation of Pb isotopes during zircon dating: Geostandards and Geoanalytical Research, v. 33, p. 145–168.

Tanaka, T, Togashi, S et al. 2000, JNdi-1: a neodymium isotopic reference in consistency with LaJolla neodymium: Chemical Geology, v. 168, p. 279–281.

Vermeesch, P 2012, On the visualisation of detrital age distributions: Chemical Geology, v. 312–313, p. 190–194.

Wingate, MTD, Lu, Y and Fielding, IOH 2022, Introduction to geochronology information 2022: Geological Survey of Western Australia, 8p.

Appendix 3.

U–Pb analytical data for zircons from ballast stone sample T002-23

					uncorrected data					204-corrected data									207-corrected data		
Group ID	Analysis ID	^{238}U (ppm)	^{232}Th (ppm)	$\frac{^{232}Th}{^{238}U}$	$^{238}U/^{206}Pb$	± 1σ	$^{207}Pb/^{206}Pb$	± 1σ	f204 (%)	$^{238}U/^{206}Pb\ast$	± 1σ	$^{207}Pb\ast/^{206}Pb\ast$	± 1σ	$^{238}U/^{206}Pb\ast$ date (Ma)	±1σ	$^{207}Pb\ast/^{206}Pb\ast$ date (Ma)	±1σ	Disc. (%)	f207 (%)	$^{238}U/^{206}Pb\ast$ date (Ma)	±1σ
Y	8.1	989	123	0.12	11.242	0.101	0.05956	0.00076	-0.042	11.237	0.101	0.05991	0.00080	550	5	600	29	8.4	0.130	549	5
S	89.1	335	294	0.88	10.790	0.113	0.05935	0.00106	0.000	10.790	0.113	0.05935	0.00106	571	6	580	39	1.5	0.029	571	6
S	45.1	232	36	0.16	10.666	0.123	0.05855	0.00126	0.095	10.676	0.124	0.05778	0.00148	577	6	521	56	-10.7	-0.092	578	7
S	31.1	242	111	0.46	10.631	0.120	0.05958	0.00121	0.343	10.667	0.121	0.05680	0.00185	578	6	484	72	-19.4	0.030	579	6
S	1.1	359	262	0.73	10.620	0.110	0.06020	0.00099	0.352	10.657	0.111	0.05735	0.00147	578	6	505	56	-14.5	0.106	580	6
S	5.1	444	241	0.54	10.595	0.107	0.05809	0.00100	0.133	10.609	0.107	0.05701	0.00118	581	6	492	45	-18.0	-0.162	582	6
S	59.1	331	254	0.77	10.422	0.203	0.05728	0.00112	-0.074	10.415	0.203	0.05788	0.00127	591	11	525	48	-12.5	-0.295	592	11
S	79.1	151	161	1.07	10.102	0.269	0.06010	0.00151	0.281	10.131	0.271	0.05781	0.00222	607	15	523	84	-16.1	-0.005	608	16
S	101.1	1812	302	0.17	10.062	0.086	0.06305	0.00067	0.222	10.084	0.086	0.06123	0.00078	610	5	647	27	5.8	0.355	609	5
S	2.1	291	247	0.85	9.998	0.109	0.06324	0.00110	0.183	10.017	0.110	0.06174	0.00140	613	6	665	49	7.8	0.367	612	7
S	103.1	674	496	0.74	9.944	0.093	0.06120	0.00084	-0.086	9.935	0.093	0.06190	0.00093	618	6	671	32	7.8	0.100	617	6
S	55.1	220	19	0.09	9.794	0.114	0.06161	0.00131	-0.387	9.757	0.115	0.06480	0.00206	629	7	768	67	18.1	0.120	626	7
S	100.1	852	23	0.03	9.777	0.089	0.06026	0.00078	0.000	9.777	0.089	0.06026	0.00078	628	5	613	28	-2.4	-0.052	628	6
S	62.1	156	107	0.69	9.782	0.125	0.05982	0.00145	0.254	9.807	0.127	0.05776	0.00206	626	8	521	78	-20.2	-0.106	628	8
S	60.1	163	203	1.24	9.753	0.212	0.05921	0.00150	-0.138	9.740	0.212	0.06033	0.00187	630	13	615	67	-2.4	-0.188	630	13
S	4.1	361	250	0.69	9.715	0.101	0.06023	0.00100	0.454	9.760	0.102	0.05655	0.00159	629	6	474	62	-32.7	-0.070	632	6
S	80.1	163	266	1.63	9.720	0.183	0.05911	0.00145	0.000	9.720	0.183	0.05911	0.00145	631	11	571	54	-10.5	-0.207	632	12
S	94.1	1114	527	0.47	9.675	0.086	0.06158	0.00072	0.207	9.695	0.087	0.05989	0.00087	633	5	600	32	-5.5	0.090	634	6
S	68.1	186	37	0.20	9.681	0.129	0.05851	0.00131	0.000	9.681	0.129	0.05851	0.00131	634	8	549	49	-15.4	-0.290	635	8
S	50.1	180	120	0.66	9.601	0.125	0.06282	0.00133	0.000	9.601	0.125	0.06282	0.00133	639	8	702	45	9.1	0.229	637	8
S	12.1	157	74	0.47	9.538	0.120	0.06103	0.00141	0.115	9.549	0.120	0.06009	0.00169	642	8	607	61	-5.8	-0.008	643	8
S	113.1	287	131	0.46	9.536	0.151	0.05998	0.00112	0.352	9.569	0.152	0.05712	0.00171	641	10	496	66	-29.1	-0.140	644	10
S	23.1	270	185	0.68	9.499	0.107	0.06014	0.00111	-0.201	9.480	0.108	0.06179	0.00146	646	7	667	51	3.1	-0.128	646	7
S	102.1	234	214	0.91	9.463	0.108	0.05975	0.00119	0.000	9.463	0.108	0.05975	0.00119	648	7	594	43	-8.9	-0.186	649	7
S	20.1	152	208	1.37	9.382	0.187	0.06237	0.00142	0.000	9.382	0.187	0.06237	0.00142	653	12	687	49	4.9	0.122	652	13
S	74.1	97	46	0.47	9.386	0.140	0.06157	0.00175	0.188	9.404	0.141	0.06003	0.00233	651	9	605	84	-7.7	0.023	652	10
S	106.1	211	134	0.64	9.339	0.109	0.06144	0.00125	0.343	9.371	0.111	0.05865	0.00188	654	7	554	70	-18.0	-0.003	656	8
S	63.1	203	65	0.32	9.327	0.168	0.06185	0.00130	-0.096	9.319	0.168	0.06264	0.00152	657	11	696	52	5.6	0.045	656	12
S	14.1	677	424	0.63	9.295	0.087	0.06198	0.00123	-0.081	9.288	0.087	0.06264	0.00129	659	6	696	44	5.3	0.053	658	6
S	44.1	42	24	0.57	9.211	0.185	0.06130	0.00416	1.226	9.326	0.199	0.05148	0.00712	657	13	262	318	-150.2	-0.052	665	13
S	69.1	591	98	0.17	9.180	0.134	0.06223	0.00089	0.139	9.193	0.134	0.06109	0.00106	666	9	642	37	-3.6	0.056	666	9
S	16.1	238	93	0.39	9.176	0.104	0.06178	0.00120	0.289	9.203	0.105	0.05943	0.00169	665	7	583	62	-14.1	-0.001	667	7
S	19.1	1034	78	0.08	9.106	0.110	0.06182	0.00073	-0.017	9.105	0.110	0.06196	0.00074	672	8	673	26	0.2	-0.013	672	8
S	88.1	648	383	0.59	9.086	0.087	0.05980	0.00085	-0.063	9.080	0.087	0.06032	0.00092	674	6	615	33	-9.5	-0.270	675	6
S	82.1	100	47	0.47	8.969	0.319	0.06164	0.00177	0.580	9.021	0.323	0.05693	0.00326	678	23	489	126	-38.6	-0.071	682	24
S	70.1	301	59	0.20	8.889	0.095	0.06198	0.00108	-0.059	8.883	0.095	0.06246	0.00118	688	7	690	40	0.3	-0.051	688	7
S	98.1	410	362	0.88	8.861	0.091	0.06143	0.00096	0.000	8.861	0.091	0.06143	0.00096	689	7	654	33	-5.4	-0.126	690	7
S	75.1	215	136	0.63	8.784	0.103	0.06309	0.00124	0.253	8.807	0.104	0.06102	0.00173	693	8	640	61	-8.4	0.060	695	8
S	21.1	267	77	0.29	8.272	0.091	0.06204	0.00110	0.000	8.272	0.091	0.06204	0.00110	736	8	675	38	-8.9	-0.222	737	8
S	54.1	113	58	0.51	8.137	0.114	0.06478	0.00161	0.000	8.137	0.114	0.06478	0.00161	747	10	767	52	2.6	0.075	747	10
S	71.1	383	172	0.45	7.743	0.079	0.06506	0.00096	0.082	7.750	0.079	0.06438	0.00108	782	8	754	35	-3.8	-0.026	783	8
S	87.1	403	190	0.47	7.566	0.076	0.06571	0.00092	0.035	7.568	0.076	0.06543	0.00097	800	8	788	31	-1.5	-0.012	800	8
S	38.1	379	175	0.46	7.554	0.078	0.06573	0.00095	0.119	7.563	0.078	0.06475	0.00111	801	8	766	36	-4.5	-0.014	802	8
S	24.1	368	147	0.40	7.299	0.074	0.06621	0.00093	0.293	7.321	0.075	0.06380	0.00126	825	8	735	42	-12.3	-0.058	828	8
S	34.1	286	171	0.60	7.018	0.076	0.06821	0.00101	0.043	7.021	0.076	0.06786	0.00107	858	9	864	33	0.7	0.067	858	9
S	17.1	700	135	0.19	7.018	0.066	0.06736	0.00138	-0.020	7.016	0.066	0.06753	0.00139	859	8	854	43	-0.6	-0.040	859	8
S	96.1	121	120	0.99	6.912	0.096	0.06898	0.00146	0.106	6.919	0.096	0.06810	0.00171	870	11	872	52	0.2	0.111	870	12
S	95.1	115	71	0.62	6.917	0.099	0.06467	0.00146	0.118	6.926	0.099	0.06369	0.00176	869	12	731	58	-18.9	-0.423	874	12
S	67.1	155	109	0.70	6.736	0.183	0.06986	0.00132	0.336	6.758	0.184	0.06708	0.00192	890	23	840	60	-5.9	0.134	891	23
S	93.1	103	107	1.03	6.694	0.095	0.06907	0.00154	0.237	6.710	0.096	0.06711	0.00208	896	12	841	65	-6.5	0.014	897	12
S	3.1	250	98	0.39	6.663	0.075	0.07061	0.00105	0.047	6.666	0.075	0.07022	0.00112	901	10	935	33	3.6	0.190	900	10
S	26.1	1096	548	0.50	6.644	0.059	0.06896	0.00069	0.000	6.644	0.059	0.06896	0.00069	904	8	898	21	-0.7	-0.026	904	8
S	18.1	248	101	0.41	6.534	0.073	0.07055	0.00107	0.246	6.550	0.073	0.06851	0.00141	916	10	884	43	-3.6	0.112	917	10
S	46.1	302	246	0.82	6.481	0.123	0.06858	0.00155	0.297	6.500	0.124	0.06613	0.00181	923	16	811	57	-13.8	-0.162	926	17
S	49.1	141	82	0.58	6.228	0.083	0.07107	0.00138	0.360	6.250	0.084	0.06808	0.00204	957	12	871	62	-9.8	-0.003	960	12
S	56.1	163	144	0.88	5.923	0.139	0.07006	0.00123	-0.141	5.915	0.139	0.07123	0.00148	1007	22	964	42	-4.4	-0.329	1009	23
S	35.1	118	43	0.36	6.196	0.085	0.07159	0.00229	0.378	6.219	0.086	0.06846	0.00279	961	12	882	84	-8.9	0.043	964	13
S	51.1	454	1062	2.34	6.145	0.060	0.07366	0.00087	-0.072	6.140	0.060	0.07426	0.00094	973	9	1049	25	7.2	0.267	970	9
S	112.1	76	52	0.69	6.040	0.099	0.07082	0.00172	0.303	6.058	0.100	0.06830	0.00249	985	15	878	75	-12.2	-0.154	989	15
S	92.1	179	312	1.74	6.001	0.075	0.07359	0.00122	0.196	6.013	0.076	0.07196	0.00154	992	12	985	44	-0.7	0.164	992	12
S	111.1	129	88	0.68	5.745	0.079	0.07294	0.00134	0.082	5.750	0.080	0.07225	0.00150	1034	13	993	42	-4.1	-0.100	1035	14
S	36.1	444	34	0.08	5.848	0.059	0.07331	0.00086	0.124	5.856	0.059	0.07227	0.00098	1016	10	994	27	-2.3	0.022	1017	10
S	33.1	404	184	0.46	5.965	0.064	0.07295	0.00138	0.028	5.967	0.064	0.07271	0.00140	999	10	1006	39	0.7	0.060	999	10
S	6.1	592	112	0.19	5.824	0.056	0.07278	0.00075	0.000	5.824	0.056	0.07278	0.00075	1022	9	1008	21	-1.4	-0.062	1022	9
S	78.1	284	194	0.68	5.717	0.063	0.07453	0.00103	0.209	5.729	0.063	0.07278	0.00130	1037	11	1008	36	-2.9	0.077	1038	11
S	57.1	384	262	0.68	5.950	0.086	0.07320	0.00093	0.031	5.952	0.086	0.07294	0.00097	1001	13	1012	27	1.1	0.080	1001	14
S	27.1	665	321	0.48	5.844	0.115	0.07325	0.00077	0.034	5.846	0.115	0.07297	0.00080	1018	19	1013	22	-0.5	0.012	1018	19

					uncorrected data							204-corrected data										207-corrected data		
Group ID	Analysis ID	^{238}U (ppm)	^{232}Th (ppm)	$\frac{^{232}Th}{^{238}U}$	^{238}U/^{206}Pb	± 1σ	^{207}Pb/^{206}Pb	± 1σ	f204 (%)	^{238}U/^{206}Pb*	± 1σ	^{207}Pb*/^{206}Pb*	± 1σ	^{238}U/^{206}Pb* date (Ma)	±1σ	^{207}Pb*/^{206}Pb* date (Ma)	±1σ	Disc. (%)	f207 (%)	^{238}U/^{206}Pb* date (Ma)	±1σ
S	53.1	353	45	0.13	5.891	0.061	0.07246	0.00092	-0.062	5.887	0.061	0.07298	0.00100	1011	10	1013	28	0.2	-0.053	1011	10
S	108.1	504	91	0.18	5.616	0.056	0.07382	0.00085	0.097	5.622	0.056	0.07301	0.00095	1055	10	1014	26	-4.1	-0.090	1057	10
S	48.1	577	315	0.55	5.899	0.057	0.07291	0.00080	-0.039	5.896	0.057	0.07323	0.00083	1010	9	1020	23	1.0	0.008	1009	9
S	15.1	193	149	0.77	5.764	0.068	0.07291	0.00114	-0.055	5.761	0.068	0.07337	0.00123	1032	11	1024	34	-0.8	-0.090	1032	12
S	66.1	304	403	1.33	5.786	0.063	0.07359	0.00099	0.000	5.786	0.063	0.07359	0.00099	1028	10	1030	27	0.2	0.011	1028	11
S	13.1	227	142	0.63	5.652	0.064	0.07453	0.00113	-0.052	5.649	0.064	0.07497	0.00121	1051	11	1068	32	1.6	0.026	1050	12
S	91.1	471	80	0.17	5.413	0.054	0.07618	0.00123	0.044	5.415	0.054	0.07581	0.00125	1092	10	1090	33	-0.2	0.033	1093	11
S	97.1	687	148	0.21	5.402	0.051	0.07652	0.00076	0.030	5.404	0.051	0.07627	0.00078	1095	9	1102	20	0.7	0.066	1094	10
S	83.1	203	61	0.30	5.291	0.063	0.07814	0.00115	0.101	5.296	0.063	0.07729	0.00130	1115	12	1129	33	1.2	0.168	1114	13
S	10.1	305	300	0.99	4.199	0.045	0.08880	0.00093	0.047	4.201	0.045	0.08839	0.00097	1376	13	1391	21	1.0	0.131	1375	14
S	84.1	299	79	0.27	4.117	0.045	0.08983	0.00096	0.025	4.118	0.045	0.08962	0.00098	1401	14	1417	21	1.1	0.119	1400	15
S	40.1	186	96	0.52	3.754	0.045	0.09371	0.00110	-0.035	3.753	0.045	0.09401	0.00114	1523	16	1508	23	-1.0	-0.126	1524	18
S	105.1	97	86	0.89	3.278	0.048	0.10073	0.00286	-0.186	3.272	0.048	0.10234	0.00300	1719	22	1667	54	-3.1	-0.563	1725	26
S	76.1	127	84	0.66	3.074	0.042	0.10971	0.00129	0.207	3.081	0.042	0.10790	0.00152	1812	22	1764	26	-2.7	-0.164	1818	25
S	61.1	160	54	0.34	2.976	0.037	0.11521	0.00117	0.092	2.979	0.038	0.11441	0.00126	1866	21	1871	20	0.2	0.129	1865	23
S	28.1	380	576	1.52	2.893	0.030	0.11622	0.00087	0.038	2.894	0.030	0.11589	0.00089	1913	17	1894	14	-1.0	-0.128	1916	20
S	85.1	474	503	1.06	2.960	0.030	0.11623	0.00083	0.033	2.961	0.030	0.11594	0.00085	1876	16	1895	13	1.0	0.189	1873	19
S	30.1	1512	244	0.16	2.883	0.025	0.11788	0.00063	0.058	2.884	0.025	0.11737	0.00064	1919	15	1917	10	-0.1	0.039	1919	17
S	65.1	689	30	0.04	2.918	0.027	0.11978	0.00075	0.000	2.918	0.027	0.11978	0.00075	1900	16	1953	11	2.7	0.455	1892	18
S	86.1	313	36	0.11	2.932	0.045	0.12106	0.00096	0.050	2.934	0.045	0.12063	0.00099	1891	25	1965	15	3.8	0.688	1880	29
S	110.1	666	170	0.26	2.873	0.027	0.12116	0.00106	-0.014	2.873	0.027	0.12129	0.00107	1925	16	1975	16	2.5	0.420	1918	18
S	7.1	337	200	0.59	2.756	0.029	0.12240	0.00154	0.013	2.756	0.029	0.12229	0.00154	1995	18	1990	22	-0.3	-0.037	1996	21
S	9.1	122	89	0.73	2.874	0.039	0.12386	0.00134	-0.038	2.873	0.039	0.12419	0.00138	1925	23	2017	20	4.6	0.775	1912	26
S	81.1	87	112	1.28	2.582	0.040	0.13116	0.00159	0.208	2.587	0.040	0.12933	0.00184	2107	28	2089	25	-0.8	0.033	2110	34
S	104.1	84	66	0.79	2.553	0.040	0.13476	0.00163	0.260	2.559	0.041	0.13247	0.00193	2126	29	2131	26	0.2	0.307	2125	35
S	77.1	342	254	0.74	2.537	0.026	0.13467	0.00093	-0.013	2.537	0.026	0.13478	0.00094	2142	19	2161	12	0.9	0.183	2139	23
S	32.1	362	271	0.75	2.082	0.021	0.16859	0.00094	0.027	2.082	0.022	0.16835	0.00095	2528	22	2541	9	0.5	0.219	2524	30
S	107.1	69	82	1.20	1.987	0.034	0.17105	0.00187	0.049	1.988	0.034	0.17061	0.00192	2627	37	2564	19	-2.5	-0.959	2649	55
S	72.1	193	164	0.85	2.034	0.025	0.17172	0.00121	0.035	2.035	0.025	0.17141	0.00123	2577	26	2571	12	-0.2	-0.045	2578	36
S	109.1	306	254	0.83	2.054	0.022	0.17508	0.00103	0.177	2.057	0.022	0.17350	0.00110	2554	23	2592	11	1.5	0.751	2542	32
S	39.1	522	87	0.17	2.074	0.020	0.17650	0.00083	-0.011	2.074	0.020	0.17660	0.00083	2537	21	2621	8	3.2	1.253	2511	28
S	73.1	210	101	0.48	2.062	0.024	0.17887	0.00118	-0.015	2.061	0.024	0.17900	0.00119	2549	25	2644	11	3.6	1.422	2519	34
S	64.1	449	358	0.80	2.056	0.021	0.18323	0.00092	0.007	2.056	0.021	0.18316	0.00092	2555	21	2682	8	4.7	1.976	2513	30
S	22.1	1380	481	0.35	2.005	0.017	0.18376	0.00066	0.041	2.006	0.017	0.18340	0.00067	2607	19	2684	6	2.9	1.276	2581	27
S	47.1	293	205	0.70	1.868	0.020	0.18838	0.00102	0.000	1.868	0.020	0.18838	0.00102	2764	25	2728	9	-1.3	-0.658	2778	39
S	11.1	117	106	0.90	1.904	0.026	0.19810	0.00149	0.090	1.906	0.026	0.19729	0.00154	2719	30	2804	13	3.0	1.625	2685	45
P	37.1	2925	847	0.29	12.673	0.109	0.06022	0.00063	0.060	12.681	0.110	0.05973	0.00066	489	4	594	24	17.6	0.409	488	4
D	43.1	128	292	2.28	5.425	0.073	0.07422	0.00138	0.422	5.448	0.074	0.07071	0.00210	1086	14	949	61	-14.5	-0.200	1093	14
D	42.1	123	212	1.72	5.522	0.077	0.07311	0.00135	0.251	5.536	0.078	0.07102	0.00182	1070	14	958	52	-11.8	-0.257	1076	15
D	25.1	112	62	0.55	5.661	0.080	0.07380	0.00249	0.302	5.678	0.081	0.07128	0.00289	1046	14	966	83	-8.3	-0.058	1049	15
D	58.1	425	151	0.36	5.741	0.058	0.07128	0.00091	-0.030	5.739	0.058	0.07153	0.00094	1035	10	973	27	-6.4	-0.310	1038	10
D	29.1	1079	334	0.31	5.279	0.048	0.07480	0.00067	0.065	5.283	0.048	0.07425	0.00071	1118	9	1048	19	-6.6	-0.261	1121	10
D	41.1	98	76	0.77	5.449	0.080	0.07797	0.00154	0.000	5.449	0.080	0.07797	0.00154	1086	15	1146	39	5.2	0.287	1083	15
D	52.1	492	164	0.33	2.959	0.050	0.12479	0.00140	0.010	2.960	0.050	0.12470	0.00140	1876	27	2024	20	7.3	1.293	1856	31
D	99.1	242	76	0.31	2.385	0.043	0.16002	0.00196	0.015	2.385	0.043	0.15989	0.00196	2257	34	2455	21	8.0	2.389	2212	43
D	90.1	448	24	0.05	2.106	0.039	0.19160	0.00099	0.000	2.106	0.039	0.19160	0.00099	2505	38	2756	9	9.1	3.836	2425	51

NOTES: Group ID: Y, youngest detrital zircon; S, older detrital zircons; P, radiogenic-Pb loss; D, U/Pb date >1000 Ma and discordance >5%. f204 and f207 are the fractions of common ^{206}Pb in total ^{206}Pb, determined by the 204- and 207-methods, respectively. Pb*, radiogenic Pb (i.e. corrected for common Pb). Disc., discordance = 100 × (1-[(^{238}U/^{206}Pb* date)-(^{207}Pb*/^{206}Pb* date)]/(^{207}Pb*/^{206}Pb* date)), based on 204-corrected data. All uncertainties are 1 sigma, and U/Pb ratios and dates include calibration and reproducibility uncertainties.

Appendix 4.

Whole-rock geochemistry of ballast stone samples

Method	XRF	XRF	XRF	XRF	XRF	XRF	XRF	XRF	XRF	XRF	XRF	XRF
Species	SiO_2	Al_2O_3	CaO	$Fe_2O_3^T$	K_2O	MgO	Na_2O	P_2O_5	SO_3	TiO_2	MnO	BaO
Unit	(%)	(%)	(%)	(%)	(%)	(%)	(%)	(%)	(%)	(%)	(%)	(%)
Detection limit	0.01	0.01	0.01	0.01	0.001	0.01	0.01	0.001	0.01	0.01	0.01	0.01
T002-23	76.44	11.03	0.85	3.10	1.82	1.34	3.37	0.157	0.01	0.52	0.05	0.05
TR3211-1	61.04	17.06	1.00	7.89	3.86	3.66	2.01	0.194	0.01	0.87	0.12	0.06
TR3211-12	64.37	16.39	1.06	5.91	3.98	3.01	2.56	0.177	0.01	0.74	0.08	0.08
TR3211-15	69.06	13.52	2.38	5.31	2.50	1.73	2.83	0.284	0.01	1.08	0.10	0.07
T003-22	72.56	12.45	1.02	4.37	3.12	1.57	3.20	0.165	0.05	0.58	0.05	0.08
T003-22 (Rpt)	72.58	12.41	1.01	4.37	3.12	1.56	3.20	0.162	0.04	0.58	0.05	0.07

Method	XRF	TGA	LA	LA	LA	LA	LA	LA	LA	LA	LA	LA
Species	Cl	LOI	Ag	As	Ba	Be	Bi	Cd	Ce	Co	Cr	Cs
Unit	(%)	(%)	(ppm)	(ppm)	(ppm)	(ppm)	(ppm)	(ppm)	(ppm)	(ppm)	(ppm)	(ppm)
Detection limit	0.001	0.01	0.1	0.2	0.5	0.2	0.02	0.1	0.02	0.1	1	0.01
T002-23	0.014	1.20	-0.1	3.2	442	1.8	0.14	-0.1	72.8	9.1	120	3.12
TR3211-1	0.002	2.48	-0.1	25.2	576	2.8	0.36	-0.1	83.2	14.3	110	9.46
TR3211-12	0.006	1.64	-0.1	1.6	730	2.8	0.12	-0.1	71.9	18.2	87	10.90
TR3211-15	0.024	1.20	-0.1	11.4	638	2.0	0.12	0.2	108.0	11.0	139	4.67
T003-22	0.006	0.87	-0.1	19.6	726	1.8	0.08	-0.1	48.1	10.4	121	6.58
T003-22 (Rpt)	0.007	0.87	-0.1	18.8	722	1.8	0.08	-0.1	46.9	11.5	123	6.38

Method	LA	LA	LA	LA	LA	LA	LA	LA	LA	LA	LA	LA
Species	Cu	Dy	Er	Eu	Ga	Gd	Ge	Hf	Ho	In	La	Lu
Unit	(ppm)	(ppm)	(ppm)	(ppm)	(ppm)	(ppm)	(ppm)	(ppm)	(ppm)	(ppm)	(ppm)	(ppm)
Detection limit	2	0.01	0.01	0.01	0.1	0.01	0.05	0.01	0.01	0.05	0.01	0.01
T002-23	16	4.61	2.55	1.21	13.2	5.13	1.05	7.94	0.87	-0.05	39.0	0.35
TR3211-1	34	6.90	3.96	1.67	24.3	7.05	1.65	5.17	1.33	0.10	42.6	0.52
TR3211-12	28	5.58	3.31	1.29	22.7	6.03	1.65	6.27	1.19	0.05	36.0	0.46
TR3211-15	20	8.59	5.08	2.02	17.4	9.16	1.35	14.80	1.71	-0.05	58.2	0.76
T003-22	16	4.77	2.64	1.08	16.3	4.62	1.10	5.46	0.90	-0.05	23.7	0.37
T003-22 (Rpt)	16	4.23	2.56	1.19	16.0	4.47	1.15	5.16	0.92	0.05	23.6	0.38

Method	LA	LA	LA	LA	LA	LA	LA	LA	LA	LA	LA	LA
Species	Mn	Mo	Nb	Nd	Ni	Pb	Pr	Rb	Re	Sb	Sc	Se
Unit	(ppm)	(ppm)	(ppm)	(ppm)	(ppm)	(ppm)	(ppm)	(ppm)	(ppm)	(ppm)	(ppm)	(ppm)
Detection limit	1	0.2	0.01	0.01	2	1	0.01	0.05	0.01	0.1	0.1	5
T002-23	408	0.2	10.6	34.2	22	25	8.61	79.4	-0.01	1.1	5.3	-5
TR3211-1	943	0.8	16.7	41.2	44	26	10.30	173.0	-0.01	1.2	15.9	-5
TR3211-12	685	0.2	16.2	33.3	38	21	8.86	184.0	-0.01	1.2	12.0	-5
TR3211-15	793	0.4	20.2	55.8	28	15	14.10	98.4	-0.01	1.9	13.5	-5
T003-22	439	0.4	11.7	23.9	26	13	6.17	106.0	-0.01	0.7	8.3	-5
T003-22 (Rpt)	440	-0.2	11.6	24.3	24	14	6.09	105.0	-0.01	0.8	8.2	-5

Method	LA	LA	LA	LA	LA	LA	LA	LA	LA	LA	LA	LA
Species	Sm	Sn	Sr	Ta	Tb	Te	Th	Ti	Tl	Tm	U	V
Unit	(ppm)	(ppm)	(ppm)	(ppm)	(ppm)	(ppm)	(ppm)	(ppm)	(ppm)	(ppm)	(ppm)	(ppm)
Detection limit	0.01	0.2	0.1	0.01	0.01	0.2	0.01	1	0.2	0.01	0.01	0.1
T002-23	6.23	2.2	160	0.81	0.81	-0.2	11.0	3270	0.4	0.38	2.86	51.4
TR3211-1	8.27	4.8	84	1.23	1.18	0.4	13.5	5390	0.8	0.56	3.62	142.0
TR3211-12	7.00	4.6	121	1.25	0.98	-0.2	13.5	4510	0.8	0.51	3.44	95.0
TR3211-15	11.20	3.0	266	1.53	1.44	-0.2	18.9	6800	0.4	0.77	4.22	94.1
T003-22	5.19	2.6	245	0.90	0.72	0.6	9.0	3590	0.6	0.39	2.06	76.3
T003-22 (Rpt)	5.05	2.6	243	0.89	0.72	0.2	8.7	3590	0.6	0.39	2.01	76.5

Method	LA	LA	LA	LA	LA		LA		LA		LA
Species	W	Y	Yb	Zn	Zr		$^{206}Pb/^{204}Pb$		$^{207}Pb/^{204}Pb$		$^{208}Pb/^{204}Pb$
Unit	(ppm)	(ppm)	(ppm)	(ppm)	(ppm)		Ratio		Ratio		Ratio
Detection limit	0.5	0.02	0.01	5	0.5		–		–		–
T002-23	3.0	23.7	2.38	60	291		18.467		15.735		38.810
TR3211-1	3.5	35.4	3.65	130	176		18.953		15.834		39.110
TR3211-12	3.5	30.4	3.25	100	211		18.822		15.618		38.593
TR3211-15	3.0	46.0	4.99	75	539		19.436		15.510		39.383
T003-22	2.0	23.1	2.70	65	192		18.752		15.480		38.370
T003-22 (Rpt)	1.5	22.8	2.61	65	187		18.519		15.474		37.501

NOTES: XRF, X-ray fluorescence spectrometry of fused bead with lithium borate flux (XRF202); LA, laser ablation inductively coupled plasma mass spectrometry (LA-ICP-MS) of fused bead (LA101); TGA, Robotic thermo-gravimetric analysis of loss on ignition (LOI), with mass loss measured at 1000°C (ROBGTA).

Appendix 5.

Sm–Nd data for ballast stone samples and rocks in southwestern England

Sample ID or Rock unit	Sm (ppm)	Nd (ppm)	$^{143}Nd/^{144}Nd$	2 s.e.	$^{147}Sm/^{144}Nd$	$\varepsilon_{Nd(580\ Ma)}$	2 s.e.	T_{DM} (Ma)	T_{DM}^2 (Ma)
Ballast stone samples									
T003-22	4.7	22.8	0.512075	0.000007	0.1257	-5.6	0.1	1882	1689
TR3211-15	9.8	50.1	0.512013	0.000010	0.1183	-6.3	0.2	1833	1738
T002-23	6.1	32.3	0.511932	0.000011	0.1134	-7.5	0.2	1866	1830
Southwestern England sedimentary rocks									
Mylor Slate	8.1	43.9	0.511939	–	0.1113	-7.2	–	1819	1808
"	7.8	45.1	0.511943	–	0.1049	-6.7	–	1707	1766
"	8.2	42.5	0.511963	–	0.1170	-7.2	–	1888	1804
"	9.8	49.8	0.511971	–	0.1183	-7.1	–	1901	1800
"	8.2	43.7	0.511903	–	0.1139	-8.1	–	1920	1875
"	6.5	34.2	0.511963	–	0.1152	-7.0	–	1853	1794
Meadfoot Gp	8.2	44.9	0.511977	–	0.1109	-6.4	–	1756	1750
"	8.9	41.5	0.512218	–	0.1287	-3.1	–	1693	1496
Porthtowan Fm	9.6	52.5	0.511888	–	0.1103	-8.1	–	1876	1877
"	7.0	36.6	0.511913	–	0.1161	-8.1	–	1948	1873
"	5.6	28.9	0.511915	–	0.1163	-8.1	–	1949	1871
"	6.1	31.2	0.512082	–	0.1186	-5.0	–	1730	1639
"	5.9	32.7	0.512208	–	0.1096	-1.8	–	1398	1404
Kate Brook Slate	9.1	48.1	0.511997	–	0.1149	-6.3	–	1796	1743
"	7.9	44.5	0.511979	–	0.1078	-6.2	–	1702	1730
"	7.8	42.3	0.512006	–	0.1119	-5.9	–	1730	1713
"	6.1	33.0	0.511990	–	0.1119	-6.3	–	1754	1736

NOTES: Data for southwestern England sedimentary rocks are from Darbyshire and Shepherd (1994). s.e., standard error; T_{DM}, single-stage depleted mantle model age; T_{DM}^2, two-stage depleted mantle model age. Values for ε_{Nd} and model ages are calculated at 580 Ma. Parameters $(^{147}Sm/^{144}Nd)_{DM}$ = 0.2136, $(^{143}Nd/^{144}Nd)_{DM}$ = 0.513163, $(^{147}Sm/^{144}Nd)_{CHUR}$ = 0.1960, $(^{143}Nd/^{144}Nd)_{CHUR}$ = 0.512630; decay constant of ^{147}Sm = 6.54 x 10^{-12} a^{-1}. The $^{147}Sm/^{144}Nd$ of average continental crust is assumed to be 0.11.

Access GSWA products

All products
All GSWA products are free to download as PDFs from the DMIRS eBookshop <www.dmirs.wa.gov.au/ebookshop>. View other geoscience information on our website <www.dmirs.wa.gov.au/gswa>.

Hard copies
Limited products are available to purchase as hard copies from the First Floor counter at Mineral House or via the DMIRS eBookshop <www.dmirs.wa.gov.au/ebookshop>.

Fieldnotes
Fieldnotes is a free digital-only quarterly newsletter which provides regular updates to the State's exploration industry and geoscientists about GSWA's latest programs, products and services.
Access by subscribing to the GSWA eNewsletter <www.dmirs.wa.gov.au/gswaenewsletter> or downloading the free PDF from the DMIRS eBookshop <www.dmirs.wa.gov.au/ebookshop>.

GSWA eNewsletter
The GSWA eNewsletter is an online newsletter that contains information on workshops, field trips, training and other events.
To keep informed, please subscribe <www.dmirs.wa.gov.au/gswaenewsletter>.